Report to ESA/ESRIN

on the research project:

PLATE MOTION ESTIMATES THROUGH ERS INTERFEROMETRIC SAR IMAGERY CONCERNING THE IZMIT QUAKE OF AUGUST 17, 1999

Parviz Tarikhi
Muhammad Morabbi

November 2000

PLATE MOTION ESTIMATES THROUGH ERS INTERFEROMETRIC SAR IMAGERY CONCERNING THE IZMIT QUAKE OF AUGUST 17, 1999

Parviz Tarikhi
Muhammad Morabbi
Iranian Remote Sensing Center (IRSC)
No. 22, 14th Street, Saadat-Abad
Tehran 19979, Iran

Tel: +98 21 2063207
Fax: +98 21 2064474
E-mail: irsc@www.dci.co.ir

INTRODUCTION

The entire Earth planet is prone to motion while some of its solid parts seem to be still. Ground surface fluctuates slowly, glaciers flow down the mountains gradually and tectonic plates creep gently. But suddenly rupture of a fault and tremor or the eruption of a volcano occurs in some area causing devastation, destruction, harsh damage, and life loss. To better conceive the dimensions and behavior of such catastrophes, scientists have developed a method to estimate bending and stretching of earth crust without any need to use sophisticated systems and instruments as well as laborious field work. This method is called SAR interferometry.

Presently studying and monitoring natural disasters emerges as a vital concern for sustainable development, welfare and safety of community. Over recent decades, availability of new remote sensing tools provides the possibility to monitor, manage and control of natural resources and environment among of which the disasters are of great importance. Nowadays disaster mitigation and risk management programs are meaningless without the application of remote sensing and satellite telecommunications. First attempts to this mean was carried out applying optical data collected by the medium and high resolution imaging systems. Optical data proved to have some privileges and limitations. But emerging radar imaging systems revealed that this new type of data mostly do not have the limitations of the latter. In the course of its development radar technology indicated interesting and unprecedented possibilities and potentials, one of which is Synthetic Aperture Radar (SAR) interferometry.

BACKGROUND AND CONCEPTS

The first and second European Remote Sensing (ERS) satellites are the earliest orbiting platforms which their data have been applied for SAR interferometry. Operated by the European Space Agency (ESA), ERS-1 launched in 1991. ERS-2 has followed its older mate since 1994. Canadian Radarsat-1 that is equipped with imaging radar also was launched in 1994 and the first Japanese Earth Resource Satellite (JERS-1) was orbited two years earlier in 1992. Although ERS-1, 2, and Radarsat-1 and JERS-1 are going to be retired the forthcoming satellites of ESA's ENVISAT and Canada's Radarsat-2 will substitute the earlier ones.

While the successes of satellite radar interferometry are quite recent, the first endeavors go back to decades earlier. The required data in this technique are collected by SAR system --an instrument that operates by transmitting microwave radiation to ground surface and recording back-scattered signal reflections from points on the Earth surface. The two sources of coherent radiation consist of two separate passes of satellite over a common area of the Earth surface. ERS-1 and 2 scene coverage is an area of 100sq.km. Using two radar scenes of a common area of the Earth surface collected by the satellites in two different times an interferogram of the scene can be generated through complex computerized processes from phase data of radar imagery. It consists of the fringes cycling from yellow to purple to turquoise and back to yellow. Each cycle represents a change in the ground height in the direction of platform that depends on satellite geometry. They also show phase difference between the corresponding reflected signals for each common ground point that acquired at two different satellite-passes. The fringes are generated due to slightly different imaging angles, which exists anyway since the repeated satellite orbits and the sensor pointing does not perfectly coinciding.

Interferometric data is usually used to generate digital elevation models (DEM's), deformation maps, and temporal change maps. Even thick cloud cover does not obscure such images, because water droplets and ice crystals can not impede microwave signals. Furthermore radar antennas onboard the space platforms can take images equally well during the day or night, because the system provides its own light source.

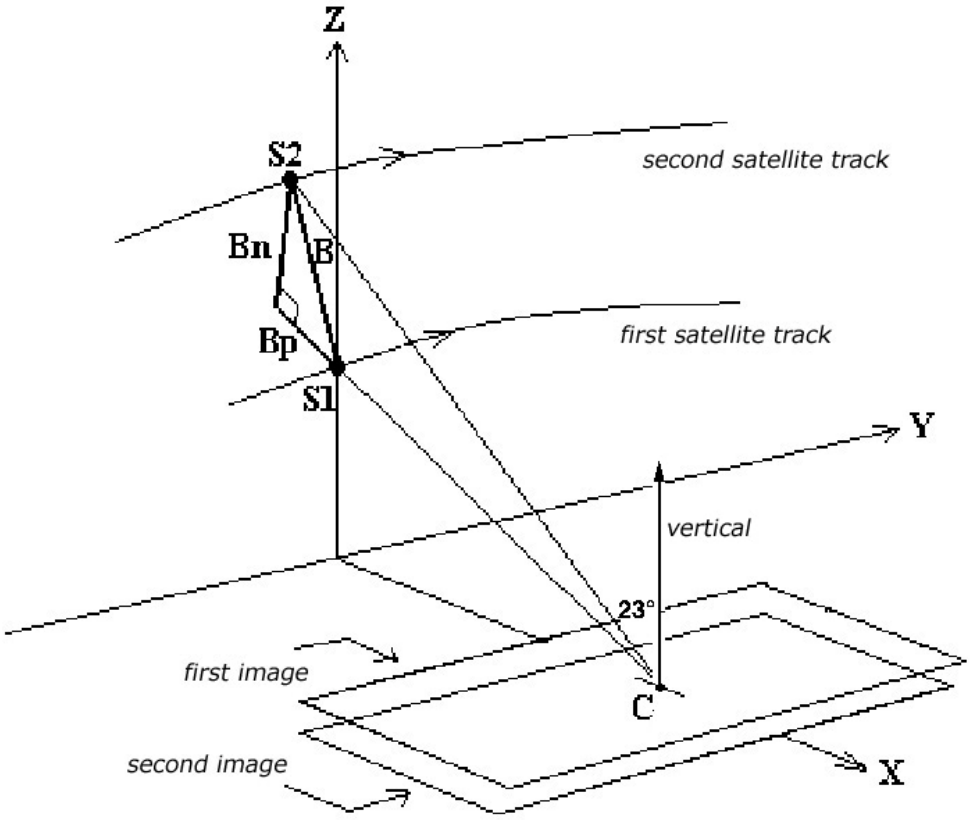

Image 1: *Satellite orbit is very important for successful application of SAR interferometry. In general a normal baseline larger than 400m is usually not suitable for interferometry. Also baselines smaller than 40m may not be suitable for DEM generation but this data are very good for differential interferometry.*

COMPARISON OF SAR AND OPTICAL TECHNIQUES

The distinction between SAR imaging and the optical systems are more profound due to the ability of SAR to operate in conditions that would cause optical instruments to fail. There are basic differences in the physical principles dominating the two approaches. Optical sensors record the radiation intensity beamed from the sun and reflected from the ground targets. Thus the intensity of the detected light characterizes each element of the resulting image or pixel. SAR antenna in contrast illuminates its target with coherent radiation the radiation in which there is definite phase relationships between different points in a cross section of the beam. Since the crests and troughs of the emitted electromagnetic wave follow a regular sinusoidal pattern, SAR can measure both the intensity and the exact point in the oscillation (phase) of returned waves.

SAR Interferometry has some similarities to stereo-optical imaging in that two images of a common area, viewed from different angles, are appropriately combined to extract the topographic information. The main difference between interferometry and stereo imaging is the way to obtain topography from stereo-optical images. Distance information is inherent in SAR data that enables the automatic generation of topography through interferometry. In other words DEMs can be generated by SAR interferometry with greater automation than optical techniques. On the other hand, using differential SAR interferometry surface deformations can be measured accurately. In addition the ability of SAR to penetrate clouds and

provide day and night operation proves that SAR interferometry has definite advantages over conventional mapping techniques.

SAR INTERFEROMETRY PRINCIPLES

In practice two SAR images of two different passes from common area are required to produce an interferometric data set from which height and other information can be extracted. To understand SAR interferometry it should be conceived that SAR measures both distance and intensity information. Distance information is encoded in phase.

Technically, the phase difference corresponding to the two passes over common locations, allow measurement of the incidence angle of the incoming radiation. Distance combined with both incidence angle and location of SAR platform on each of the two passes gives a three-dimensional location of points on the Earth surface.

Phase measuring is of great benefit since radar operates at extremely high frequencies that correspond to microwaves. In the case of ERS and Radarsat satellites for instance, the applied frequency of the system is 5.375GHz. As a result to complete one oscillation the signal travels only 5.58cm at the speed of light. If the distance from the radar antenna to the target on the ground correspond to a very large but whole number of wavelengths, the round-trip will be exactly twice. Thus when the wave returns to the satellite, it will have just completed its final cycle with unchanged phase from its original condition at the time it left. But if the distance to the ground exceeds by only 5 millimeter, the wave will have to cover an additional 1cm in round-trip distance that constitutes 18 percent of a wavelength. Consequently the phase of the reflected wave will be off by 18 percent of a cycle when it reaches the satellite. This is the amount that receiver can easily record. Therefor, the measurement of phase provides a way to estimate the distance to a target with centimeter, or even millimeter precision. Although the phase itself appears randomly every time, the phase differences between corresponding pixels in the two radar images produce a relatively direct interference pattern.

In the interferograms acquired from ERS data each color cycle corresponds to a ground displacement of 28mm or half a wavelength in the satellite's viewing or slant range direction. Simply counting the number of fringes the deformation can be estimated. In principle, if two sequential satellite images are taken from exactly the same position, phase difference for any pair of corresponding pixels should not exist. But if the scene on the ground changes a bit in the time interval of two radar scans, the phases of some pixels in the second image will shift.

Image 2: *Map of western Turkey showing the site of the Izmit quake*

IZMIT DISASTER AND AN EMPIRICAL PROJECT

On 17 August 1999 a sever quake measuring 7.8 Richter struck Western Turkey leaving very high rate of life losses and injuries in addition to homelessness and damages. The quake's epicenter was between Izmit and Bursa, 90km southeast of Istanbul on the Eastern shore of the Sea of Marmara. Nearby cities including Golcuk, Derince, Darica and Adapazari were severely devastated. Since then there have been a series of tremors in the region.

Reportedly the Izmit quake originated at a depth of 10-16km along almost vertical ruptures. Four different fault segments became active during the two consecutive shocks the first of which lasted 12 seconds and affected the western part including Golcuk, Izmit-Sapanca and Arifiye-Akyazi. After 18 minutes another shock with duration of 7 seconds originated along the Golyaka rupture to the east-northeast of Sapanca. The surface displacement reached a maximum of 5m in Arifiye while the average displacement along the active fault system was 2 to 4m.

Image 3: *The Izmit 17 August quake, scaling 7.8 Richter, leaves very high rate of life losses and injuries in addition to homelessness and damages in Western Turkey*

Izmit disaster has been monitored by the different remote sensing satellites. Not only the medium and high-resolution optical data, but also SAR data of the disaster are available thanks to the different remote sensing satellites orbiting the Earth and monitoring it.

Aiming to find the pattern of the plate motions and estimation of displacements in the concerned area through interferometric images, a small team of specialists and scientists in the Iranian Remote Sensing Center (IRSC) implemented a one-year termed research project. The required data including SAR and Landsat imagery as well as some needed software secured by the European Space Research Institute

(ESRIN) affiliated to ESA. SPOT of the Centre National des Etude Spatial (CNES) and ESA agreed to pool their space-based resources and provide timely pertinent information on parts of the Earth damaged by natural or man-made disasters, announced on 22 July at the United Nations UNISPACE III Conference at Vienna. Based on this, SAR and optical imagery as well as field data were secured as the input to the project.

The study area was the North Anatolian Fault Zone (NAFZ) that is the most active fault system in Turkey. Most of the great earthquakes have occurred in this zone. It is believed that the Sea of Marmara region is a depression (graben) that due to two fault systems running in parallel stretches slowly. Movements of the Eurasian, Arabic and African plates that activate different portions of the Anatolian fault system, explain the tectonic activity in the area.

The team used 17 scenes of SAR imagery acquired from the study area, 10 scenes before and 7 scenes after the quake. The data were mostly the Single Look Complex Image (SLCI) product while two Precision Image (PRI) Products and two raw data were available. There were also available two Landsat TM scenes before and after tremor. SCLI is a single-look complex data in slant range with no speckle reduction by multi-look processing. Phase continuity is preserved in these images, and they are particularly suitable for interferometric applications. PRI images on the other hand are speckle-reduced, ground range and system corrected imagery. They are not geocoded and terrain distortion (foreshortening and layover) has not been removed for them. In Appendix A (appendA directory) the quick looks as well as header analysis data and other parameters for each of the ERS-SAR images can be found.

Table 1: *List of the ERS-SAR data input to the project*

Data name	Date (mm/dd/yy)	Platform	Track	Frame	Orbit	Product type
B0r	06/07/1995	ERS-1	336	2781	20364	RAW
B9s	06/08/1995	ERS-2	336	2781	00691	SLCI
B8r	10/15/1998	ERS-2	336	2781	18226	RAW
B7s	12/24/1998	ERS-2	336	2781	19228	SLCI
B6s	03/04/1999	ERS-2	336	2781	20230	SLCI
B5s	03/20/1999	ERS-2	064	2781	20459	SLCI
B4p	04/05/1999	ERS-2	293	2781+2 nodes	20688	PRI
B3s	04/24/1999	ERS-2	064	2781	20960	SLCI
B2s	08/12/1999	ERS-1	157	819-4 nodes	42229	SLCI
B1s	08/13/1999	ERS-2	157	819-4 nodes	22556	SLCI
	08/17/1999	**EARTHQUAKE**				
A1p	08/23/1999	ERS-2	293	2781+2 nodes	22692	PRI
A2s	08/25/1999	ERS-1	336	2781	42408	SLCI
A3s	08/26/1999	ERS-2	336	2781	22735	SLCI
A4s	09/10/1999	ERS-1	064	2781	42637	SLCI
A5s	09/11/1999	ERS-1	064	2781	22964	SLCI
A6s	09/16/1999	ERS-1	157	819-4 nodes	42730	SLCI
A7s	09/17/1999	ERS-2	157	819-4 nodes	23057	SLCI

Table 2: *List of the Landsat TM data input to the project*

Data name	Date (mm/dd/yy)	Platform	Sensor	Details
B	03/27/1999	Landsat	TM	Path 179 Row 32
	08/17/1999	**EARTHQUAKE**		
A	08/18/1999	Landsat	TM	

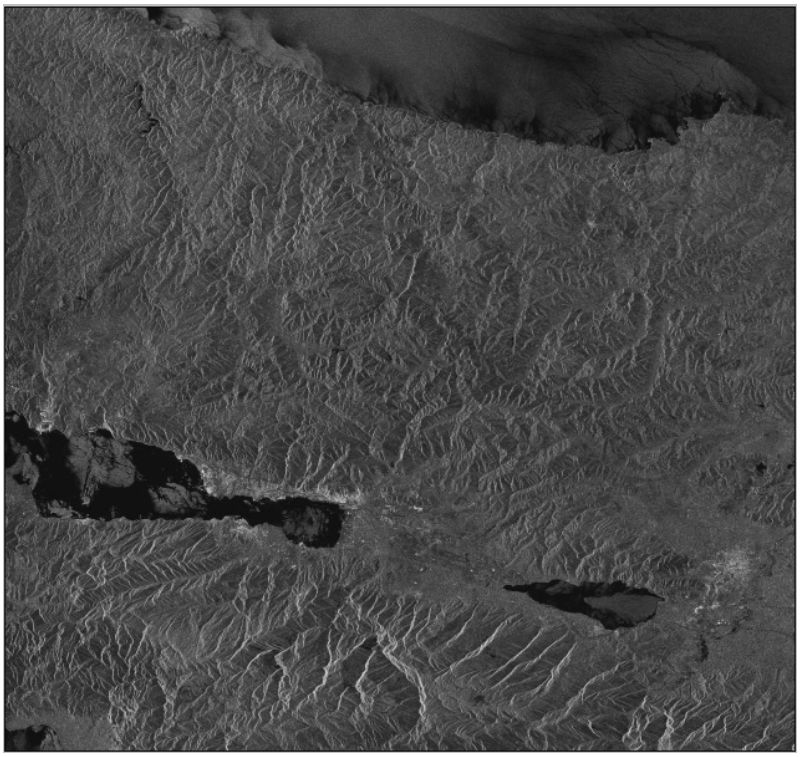

Image 4: *The full resolution image of the Izmit area acquired by ERS-2 on 13 August 1999, four days before quake.*

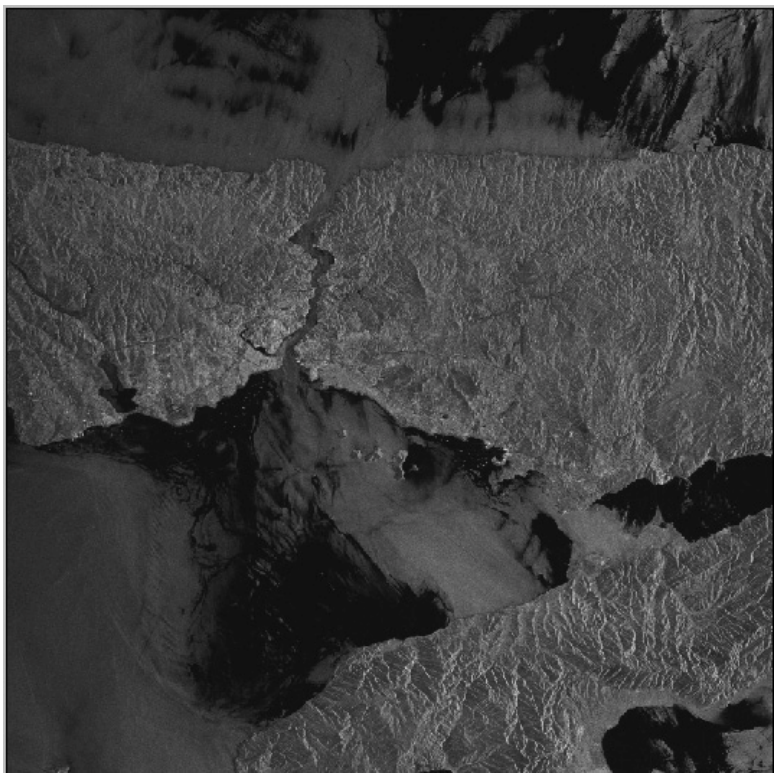

Image 5: *The full resolution image of the Istanbul area acquired by ERS-2 on 4 March 1999, five months and ten days before quake.*

To implement the research program, in addition to the noted data a variety of image analysis and GIS tools including SAR Toolbox- 6.1, Earth View Interferometric SAR- 4.4, ER-Mapper-5.5 and PhotoShop-5.5 were employed. Two linked PC computers, each with 10.2Gb of memory space – the memory space for one of the computers upgraded to 40Gb due to need for further memory space in the last month of the project-- were used to do the processing. Two full-resolution ERS-SAR images of the study area generated by SAR Toolbox are given below. Image 4 shows the full resolution image of the Izmit region acquired by ERS-2 on 13 August 1999 (four days before quake). Image 5 shows also the full resolution image of the Istanbul area acquired by ERS-2 satellite on 4 March 1999, five months and ten days before quake.

DATA INVESTIGATION AND METHODOLOGY

To approach the goal and detecting changes in the study area, it was required to investigate the appropriate SLCI and PRI image pairs to identify the coherent images. The available data were examined and studied to distinguish if there was the image pairs suitable for generating interferograms. The image pairs were classified in three groups. The first group comprised of the image pairs, one showing the scene before and the other after the quake. The second group consisted of image pairs both before the quake and the third group the image pairs of after quake. Availability of the interferograms associated to each three groups reveals the interesting points and indications that can help to understand and find out the factors and parameters involved in the occurrence of Izmit quake.

Since at the early stage the SAR Toolbox was the only applicable software, it was used to determine the baseline corresponding to each image pair. Different image pairs tried to be co-registered due to the fact that co-registration of the image pairs is a prerequisite for generating relevant interferograms, coherence images and DEMs. 39 possible pairs among the available SAR data was identified among of which 22 pairs successfully co-registered with the baselines varying from almost 10 meters to more than 1km. In Appendix B (appendB) the information on the appropriate pairs including the co-registration parameters, baseline and residual details is given. The name for each directory refers to the combination generated from two images that the first is master and the second is slave image. For instance the directory with the name b2a6 have the files related to the combination of the image b2 (from Table 1) as master and a6 as the slave image. Table 3 shows the information on the status of co-registration of ERS-SAR image pairs and their baseline concisely. The upper number in the cells of the table refers to the normal component of the baseline whereas the lower number indicates the parallel component of the baseline for the corresponding pairs. For each pair we also tried to co-register the image pairs when we changed the place of master and slave images respectively. The results are a bit different from those of relevant former pairs. One interesting case is the image pairs of 12 August 1999 and 16 September 1999 whose corresponding baseline parameters are 121.640m and 67.725m for normal and parallel components respectively. When we replace master image with slave image the values 70.912m and 66.023m are obtained for normal and parallel components respectively.

PRODUCTS

The team examined the available data using available softwares and miscellaneous information. This led to generation of two types of products including optical and SAR products. Optical products obtained using two Landsat TM scenes of the common area struck by the Izmit quake. One of the images dates 27 March 1999 and the second 18 August 1999 (a day after the quake). ER Mapper software was used to generate different combinations of two images to detect the changes.

For SAR data using SAR Toolbox we tried to generate different composites applying the available tools of the software, whereas Earth View InSAR enabled us to generate interferograms and the related products. Below some of the products can be seen. For each product the necessary details are given and discussed.

Optical products

More than 10 different products generated from the Landsat Thematic Mapper (TM) images of 27 March and 18 August. Image 6 is a false color composite generated by combining the 7, 5 and 1 bands of the Landsat TM image of 18 August 1999 a day after the earthquake. Band 7 represents the middle infrared

portion of TM sensor onboard of Landsat. It ranges from 2.08 to 2.35 micron with the spatial resolution of 30m. Band 5 is also the middle infrared TM band that ranges from 1.55 to 1.75 microns with the same spatial resolution of the band 7. Band 1 on the other hand ranging from 0.45 to 0.52 micron refers to blue color. The image shows the city of Izmit in northern shore of Izmit Bay. It seems that the bright yellow spot on top left is due to the fire caused by the explosion of the fuel tanks after quake. The dense black smoke coming up to the sky can be readily identified in left. In the Image 7 the same phenomena can be seen as a thermal anomaly. Band 6 of Landsat TM is the infrared thermal band ranging from 10.40 to 12.50 microns with the spatial resolution of 120m, and the flaming of the fuel tanks can be easily distinguished as a bright spot in the middle of the image.

Image 6: *The 7-5-1 false color composite image of 18 August 1999 a day after the quake of Izmit area that is lying on northern shore of Izmit Bay. The bright yellow spot on top left is due to the fire caused by the explosion of the fuel tanks after quake. The dense black smoke that comes up can be readily identified in left.*

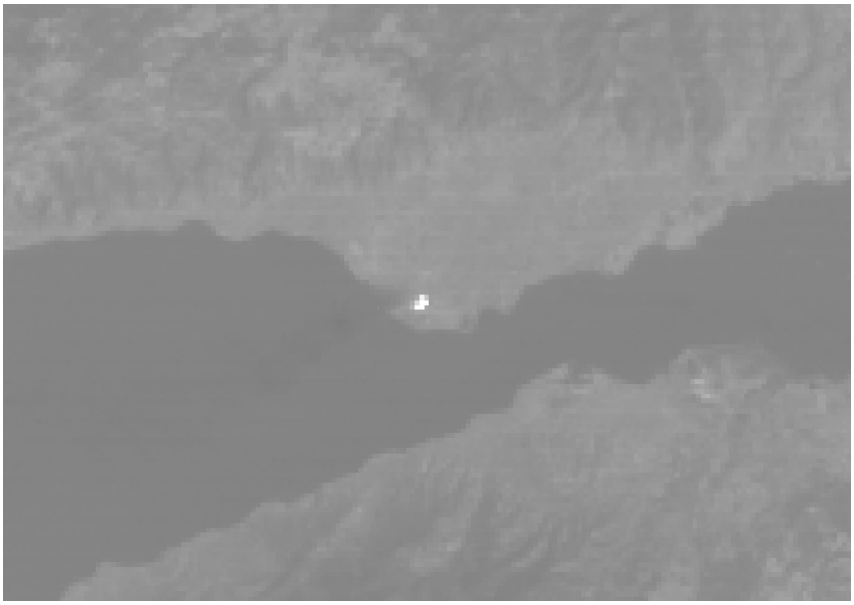

Image 7: *Band 6 of the image acquired by Landsat TM on 18 August 1999 from the Izmit area. Flaming of the fuel tanks can be easily distinguished as a bright spot in the middle of the image.*

Image 8: *This image shows the area on 27 March 1999. It is a false color composite of 4, 3, 2 TM bands.*

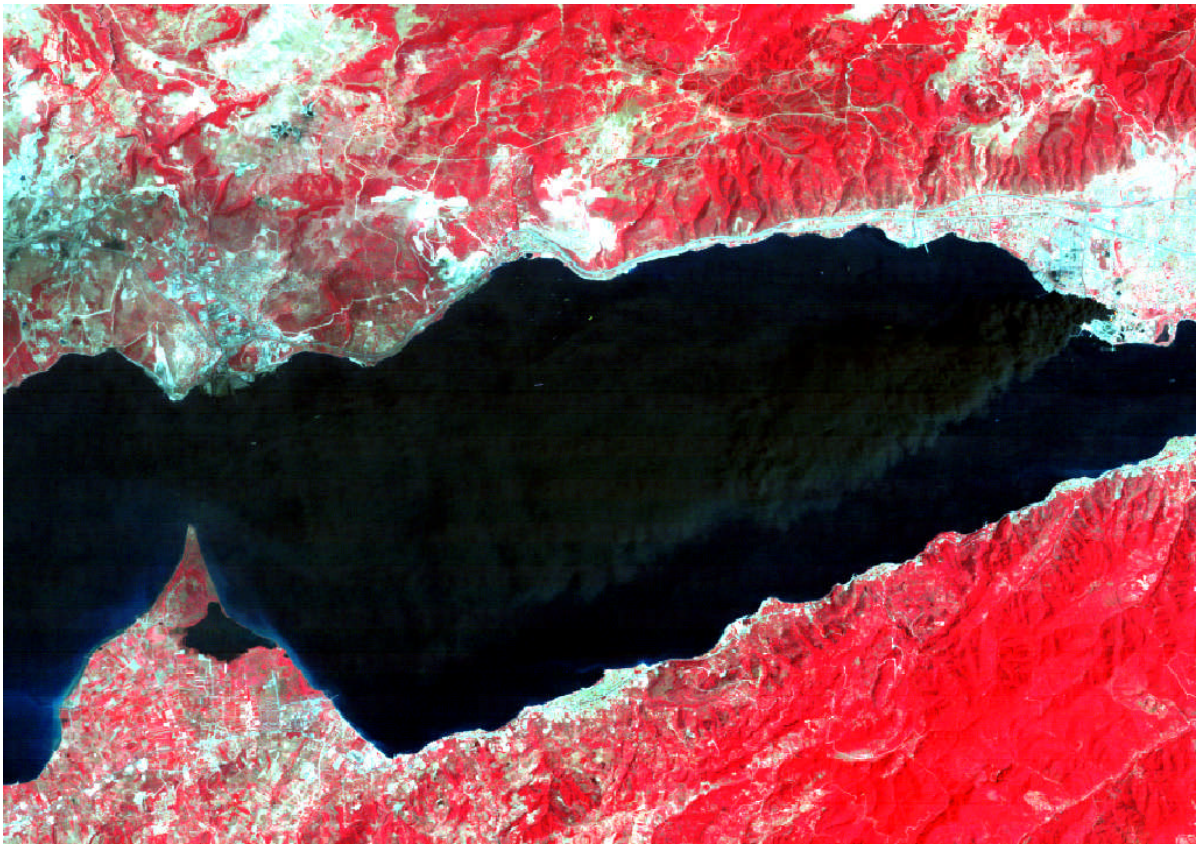

Image 9: *This image shows the area on 18 August 1999. It is a false color composite of 4, 3, 2 TM bands.*

Image 8 taken on 27 March 1999, is a false color composite that obtained combining bands 4, 3, and 2 of TM sensor. Band 4 is a near infrared band ranging from 0.76 to 0.90 micron, while band 3 or red band ranges from 0.63 to 0.69 micron and band 2 or green band ranges from 0.52 to 0.60 micron. All three bands have the spatial resolution of 30m. Image 9 that is taken on 18 august 1999 is also a false color image generated by combining TM bands 4, 3, and 2. Comparison of these two images reveals some differences around the triangle shaped peninsula as well as the Izmit Bay. In the Image 8 sea water level is lower than that of the image 9. Image 8 shows the area at the beginning of spring when the input water from the rivers is not much causing poor presence of the suspensions in the shore waters. In the Image 9 the water level is high and the presence of the suspensions in the shore waters is also increased. There is not a logical relation between the mentioned changes and the earthquake. However, the changes in the brightness of the ground features around the coastal zones of the Izmit Bay that are mainly the urban areas can be an indication of the destruction caused by the quake.

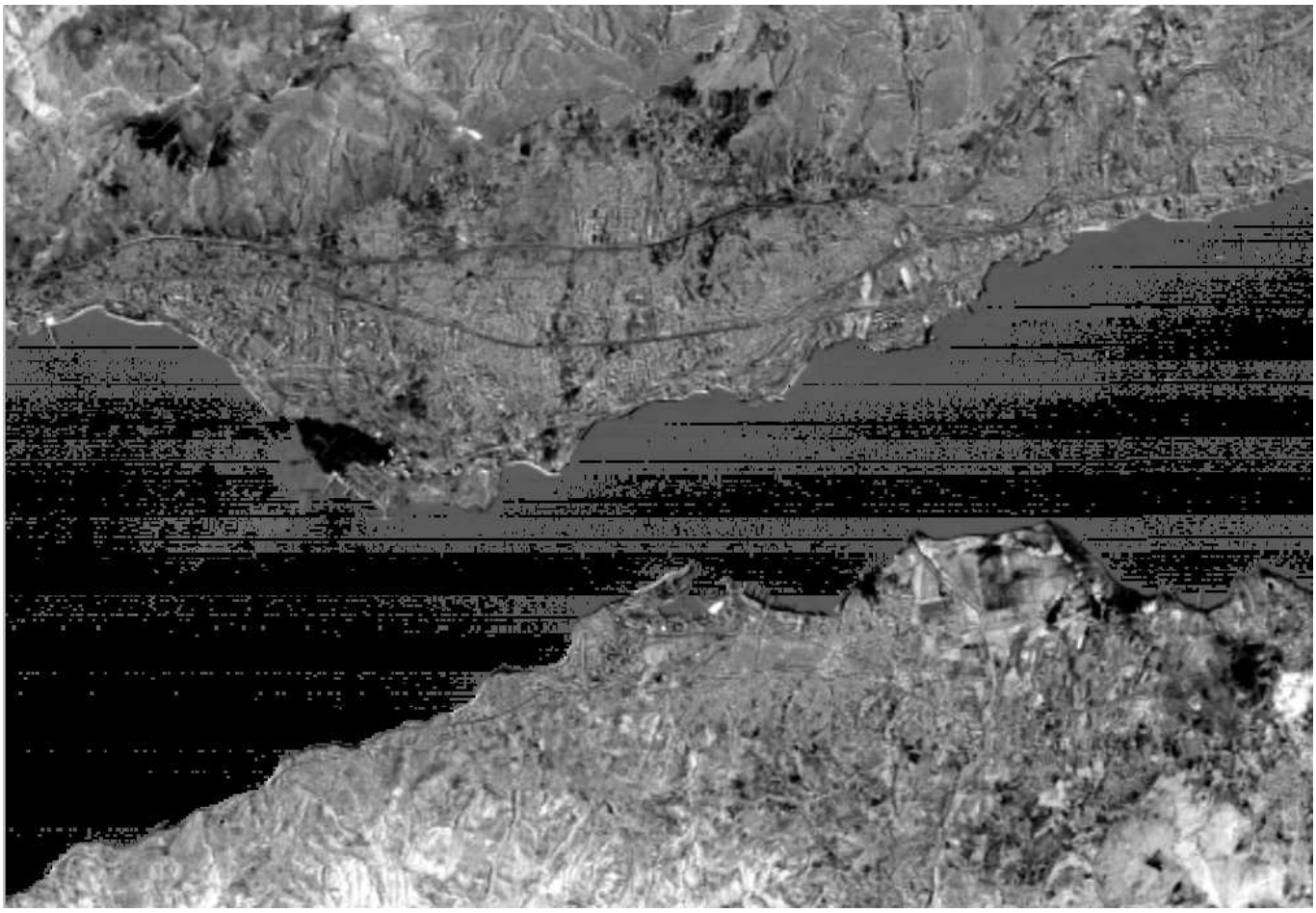

Image 9(i): *The band 3 intensity image of the images of 27 March and 18 August 1999 Landsat TM imagery*

Image 9(i) is the band-3 intensity image of the images of 27 March and 18 August 1999 Landsat TM imagery. The evident changes can be distinguished in left and northern shore of sea (the black triangular area that is due to the transgression of sea water to the urban area. The same changes can be also identified in the southern shores of the Izmit Bay at right. In the urban areas at bottom right the degree of brightness is an indication of the change due to the devastation caused by the quake.
Image 10 is the image obtained by assigning the 4, 3, and 2 bands of the image of 18 August 1999 to the intensity, hue and saturation components respectively. The red spots and areas at the top and top right and bottom left shows the changes caused by the thermal increase in those points which may be due to the fires initiated after quake.

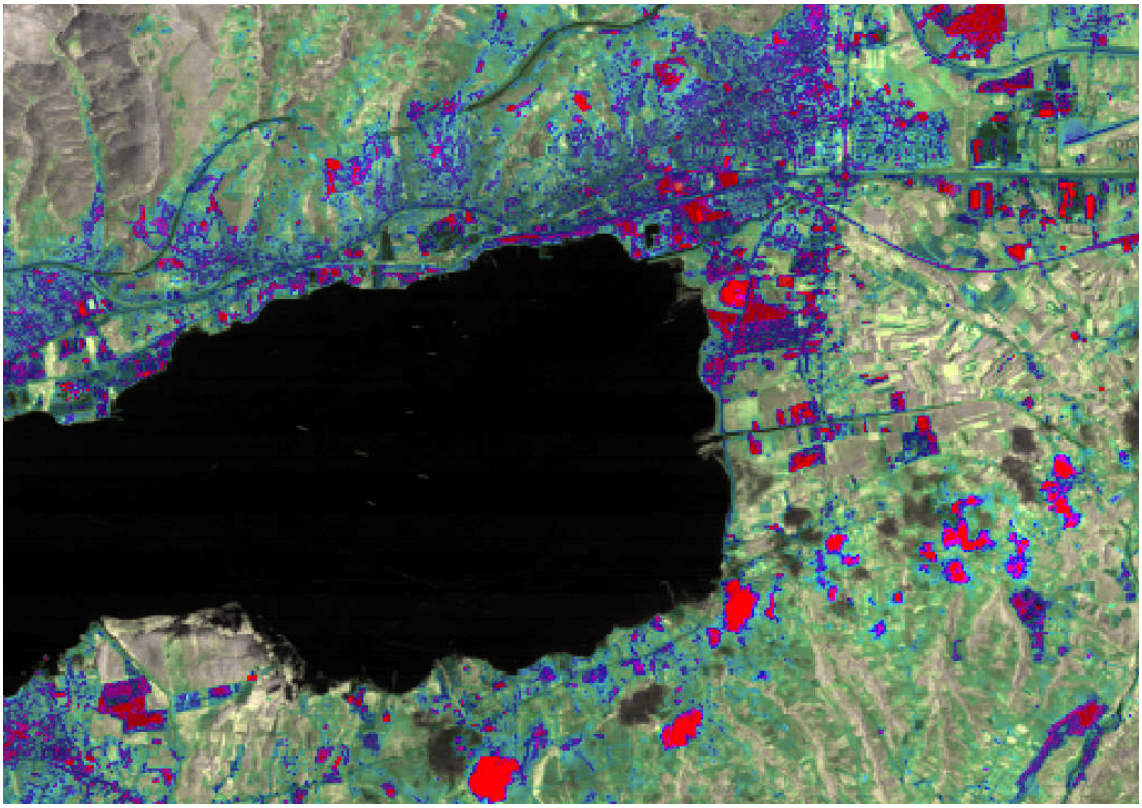

Image 10: *The image obtained through assigning the 4, 3, and 2 bands of the image of 18 August 1999 to the intensity, hue and saturation components respectively.*

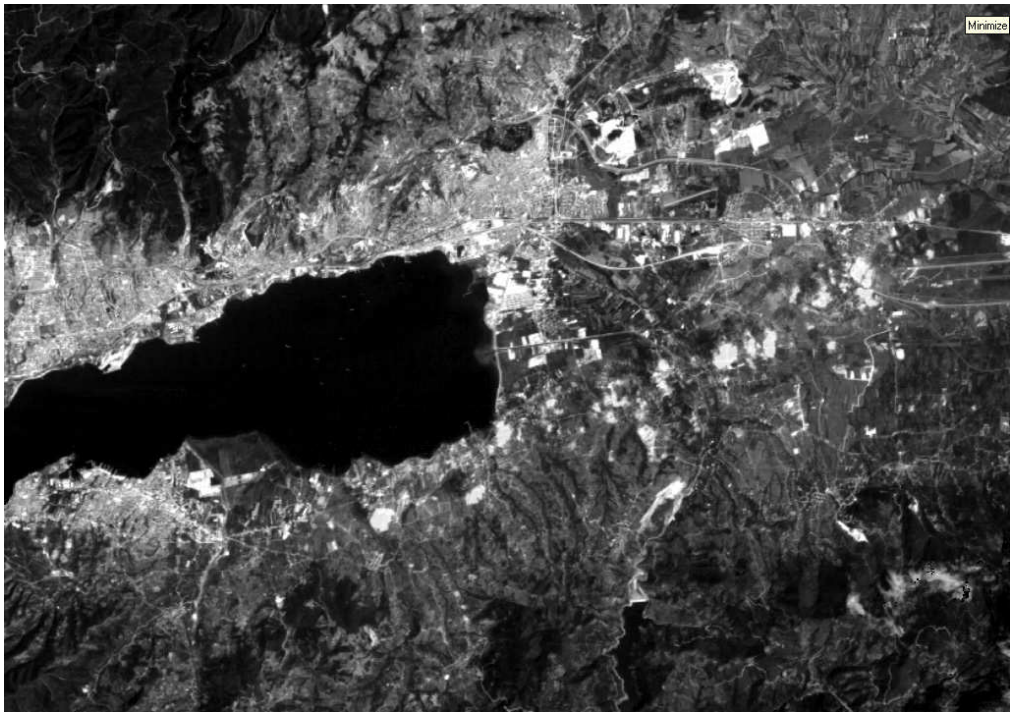

Image 11: *This image shows the second principal component obtained from the integration of the band 3 of both Landsat TM images of 27 March and 18 August 1999. The second principal component image basically indicates the areas that have changed due to the earthquake. The degree of brightness refers to the rate of the change.*

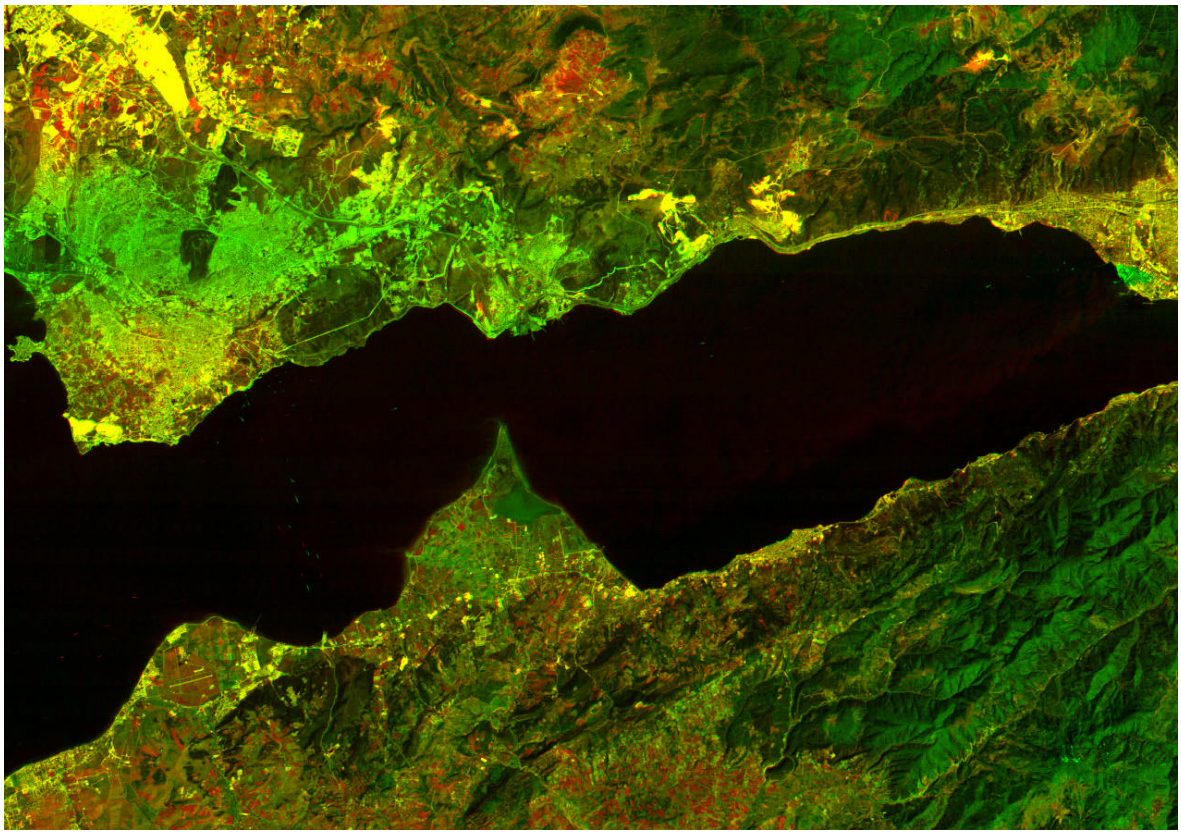

Image 12: *Red/green difference image of the area generated using the images of before and after the quake*

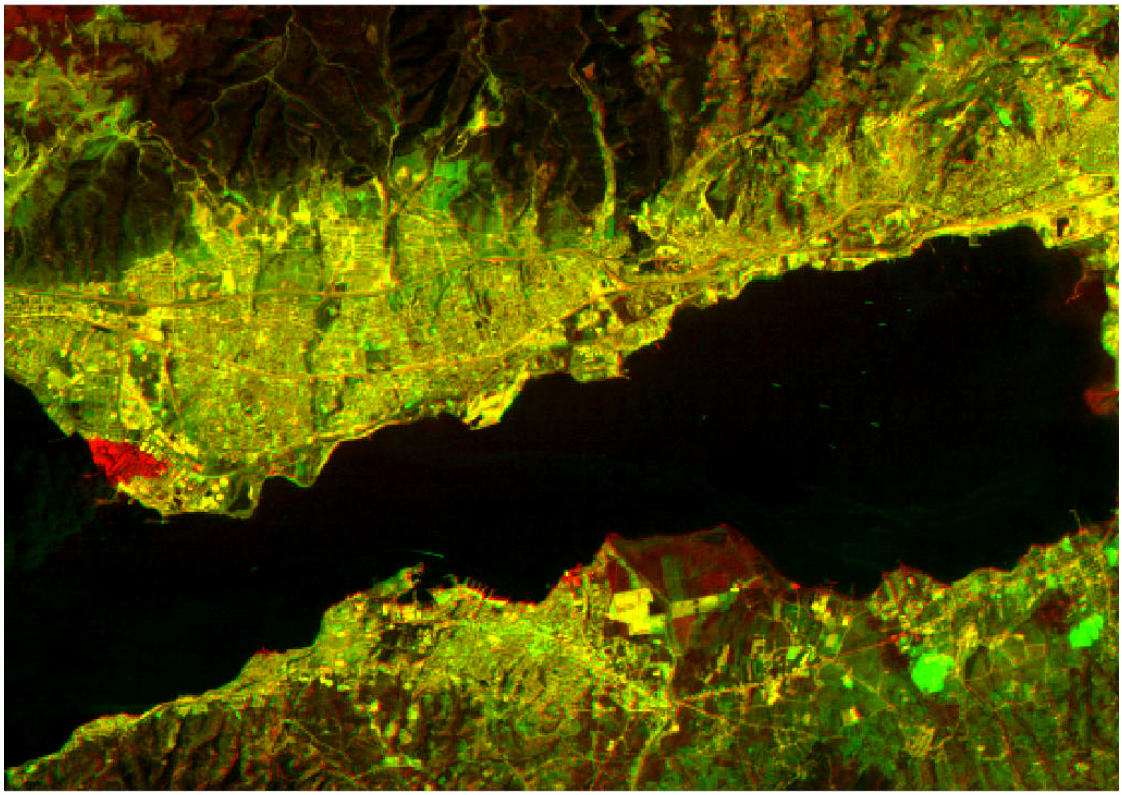

Image 13: *Red/green difference image of the area generated using the images of before and after the quake. In this image the place of the generating data sets have been exchanged.*

Image 11 shows the second principal component obtained from the integration of the band 3 of both Landsat TM images of 27 March and 18 August 1999. The second principal component image basically indicates the areas that have changed due to the earthquake. The pixels with poor correlation in the different dates appear in the second principal component image. This is exactly the case in the image 11 where the bright areas around the Izmit Bay show the lowest correlation and as a result the highest changes. The gray areas at top right and left in north of the Izmit Bay also shows the changes. The degree of brightness refers to the rate of the change.

Red/green difference image generation is one of the common techniques for the enhancement of the areas that have been changed. In this technique a data set of green color (before the quake) and the second data set of the red color (after the quake) both for band 3 is represented. The integrated output image shows the yellow shadows indicating the same reflection in two dates before and after the earthquake whereas the changed areas appear in green or red colors. Image 12 illustrates this process clearly. In these image that show the Izmit Bay and its surrounding the red pixels in the urban areas can be related to the distractions caused by the earthquake. The two considerable features in this image is the transgression effect of the sea water to the urban areas that can be distinguished in green color (top right) and the smoke from the burning site that can be seen in green color. Image 13 is the same Image 12 with the difference that the data sets have been exchanged. Consequently the transgression effect of the seawater to the urban areas can be distinguished in red color (middle left).

Image 14 is obtained from the data sets of two dates one before the quake and the other after the quake. The red color is assigned to the image of 27 March and the green and blue colors are assigned to the image of 18 August. In this image the changed sites in the urban area as well as sea attire transgression to the urban areas can be seen in red.

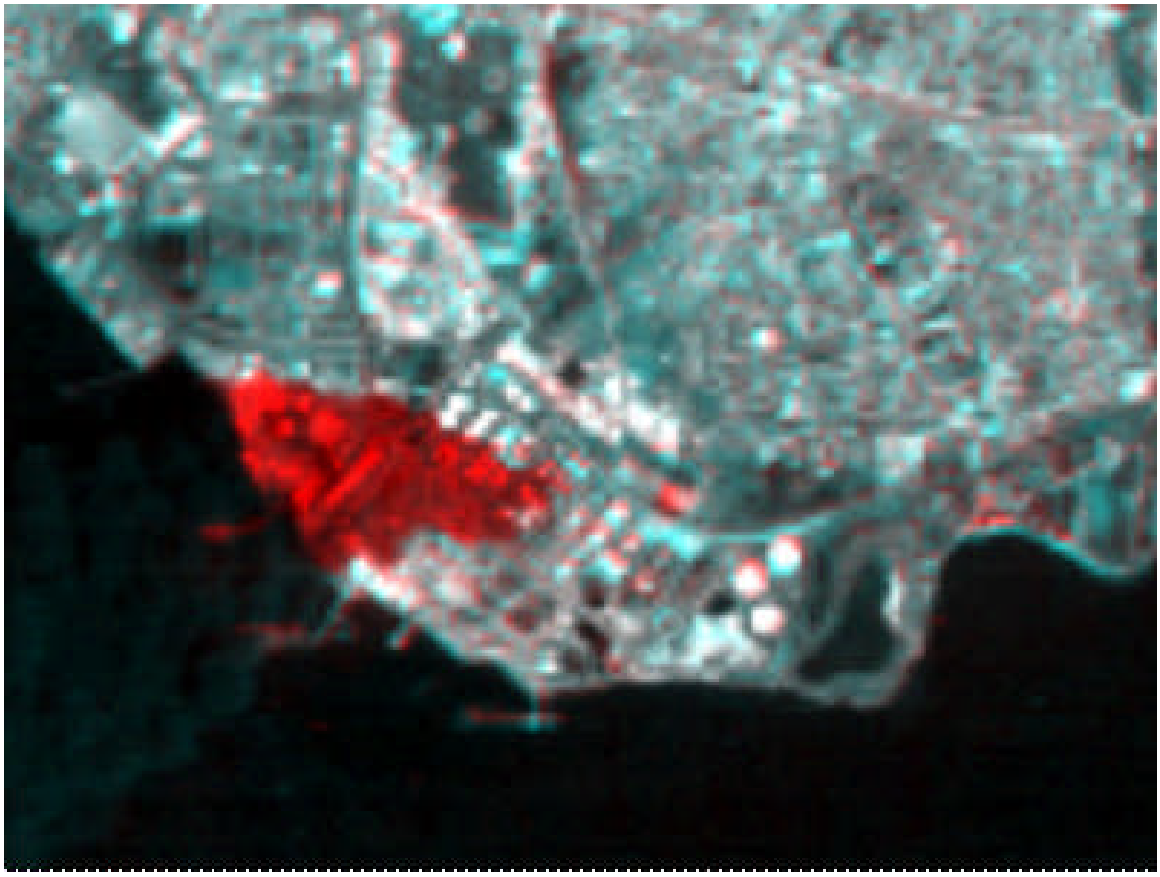

Image 14: *This Image is obtained from the data sets of two dates one before the quake and the other after the quake. In this image the changed sites in the urban area as well as sea water transgression to the urban areas can be seen in red.*

SAR products

17 SAR images the list of which is given in the Table 1 are applied. This imagery comprised of two raw images before the quake, two PRI data before and after the earthquake and 13 SLCI images -- 7 images before and 6 images after the quake. For a long term during the implementation of project SAR Toolbox was the only available software for manipulation and investigation of SAR data. It was only in the few last months of the project the team equipped with the Earth View InSAR software that enabled us to generate interferograms and the relevant products. Below some of the SAR products can be seen. Non-interferometric SAR product are given firstly and the interferometric SAR products can be seen following the non-interferometric products.

I) Non-interferometric SAR products

Image 15 is a temporal composite obtained from three images of the common area in different dates. This type of images is commonly used for change detection. Red color is assigned to the image of 13 August 1999 whereas the green and blue colors are assigned to the images of 16 and 17 September 1999 respectively. Cyan and green colors across the line joining Izmit in northeastern coast of Marmara Sea to Sapanca in south of the Lake Sapanca shows the subtle change across this line along which the most tremendous displacement has been reported. Adapazari in northeast of the Lake Sapanca, and Izmit in northeast and Golcuk in south of Izmit Bay are distinguishable.

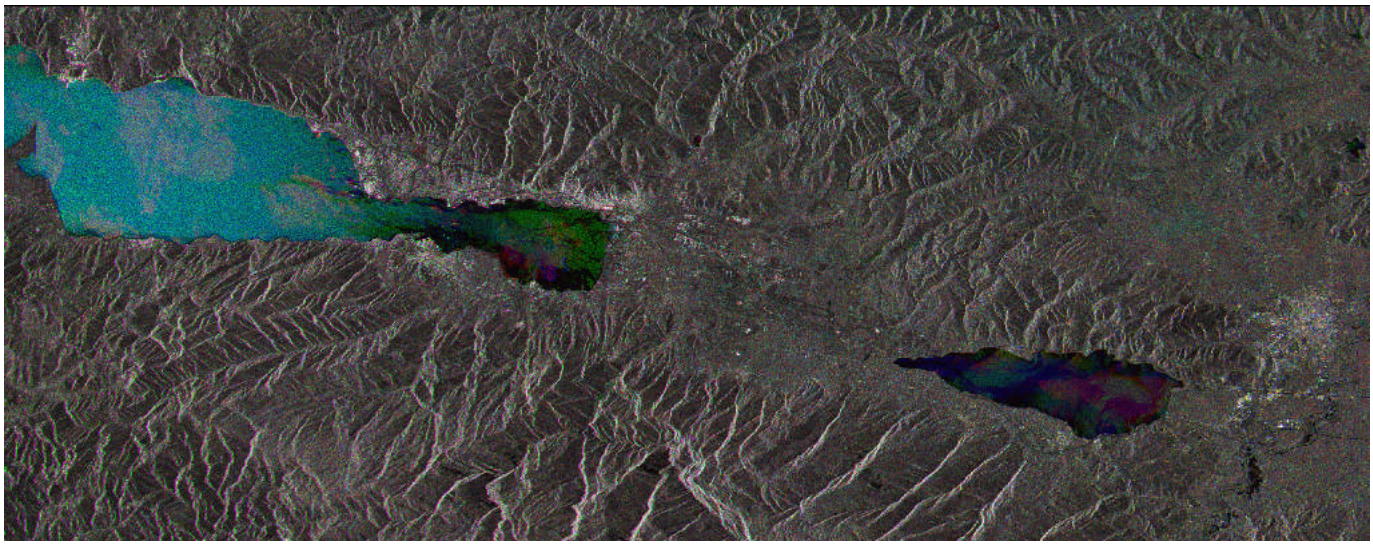

Image 15: *Temporal composite image generated from the SAR images of 13 August 1999 (red), 16 September 1999 (green) and 17 September 1999 (blue).*

Image 16 is the first principal component image generated from the images of 13 August 1999 and 16 September 1999. Image 17 is the second principal component image of the images of 13 August and 16 September 1999. The first principal component image shows the unchanged corresponding pixels in the two images while the second principal component image reveals the corresponding pixels that have changed during time. Images 16 and 17 confirm this clearly. The changes in the areas around the Izmit bay and the Lake Sapanca in the second principal component image is considerable.

Image 18 is the coherence image of the images of 13 August 1999 and 16 September 1999. There is a low correlation between two images and it is evident from the coherence image.

Image 19 obtained from the images of 13 August (4 days before the quake), 16 September (one month after the quake) 1999 and the second principal component of these two images. We have given red color to the first image and green and blue to the second image and the second principal component images respectively. Blue and yellow colors in the urban areas struck by the quake are the indication of surface disturbances. Image 20 is also obtained from the images of 13 August, 16 September 1999 and the second principal component of these two images. But in this case red color is given to the principal component image and green and blue colors are given to the images of 13 August, 16 September 1999 respectively. Red and cyan colors in the urban areas damaged by the quake indicate the changes.

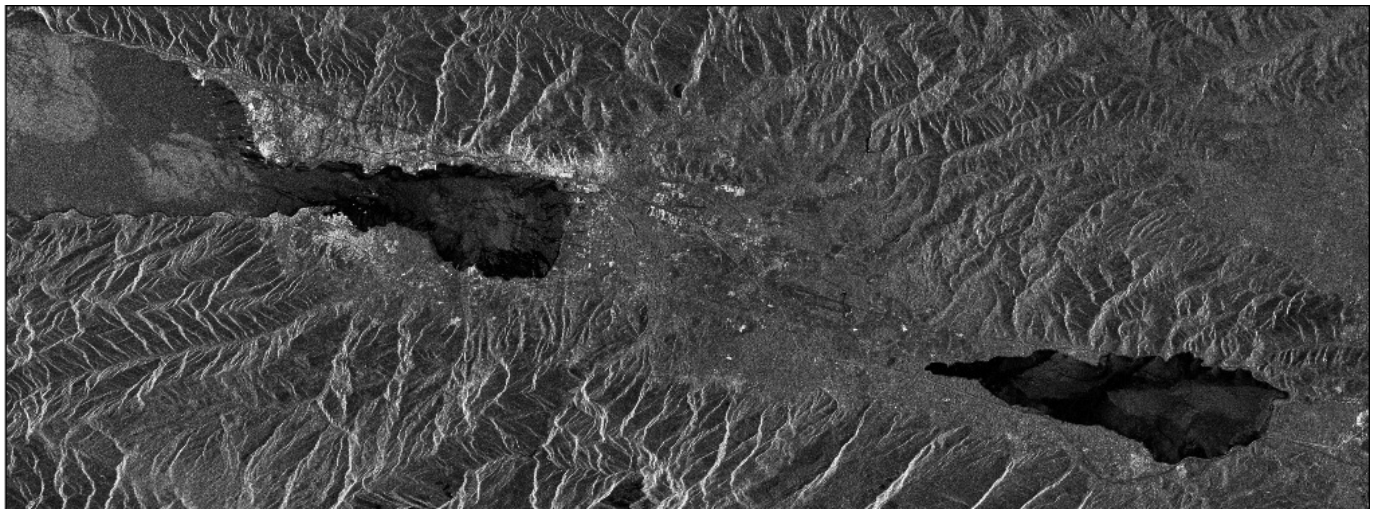

Image 16: *The first principal component image generated from the images of 13 August and 16 September 1999.*

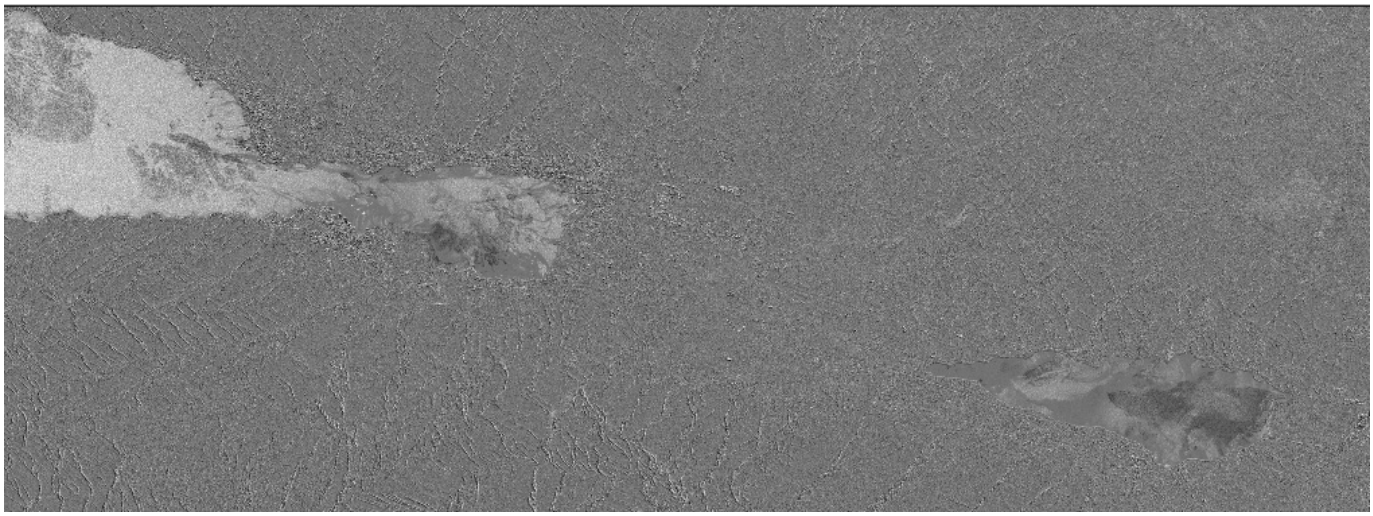

Image 17: *The second principal component image generated from the images of 13 August and 16 September 1999.*

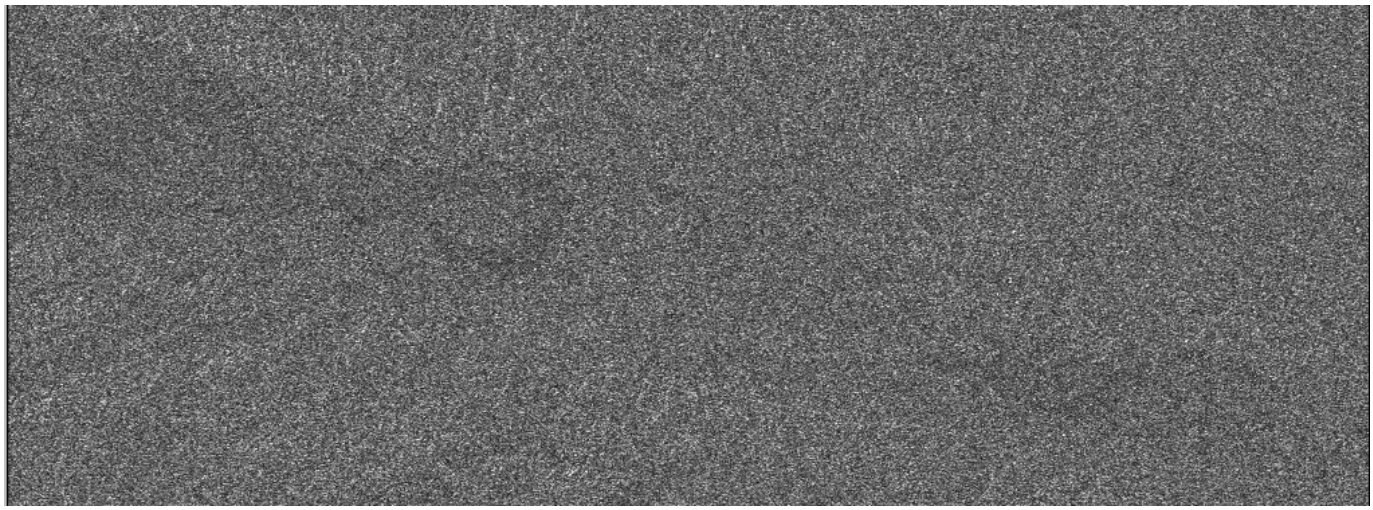

Image 18: *The coherence image of the images of 13 August and 16 September 1999.*

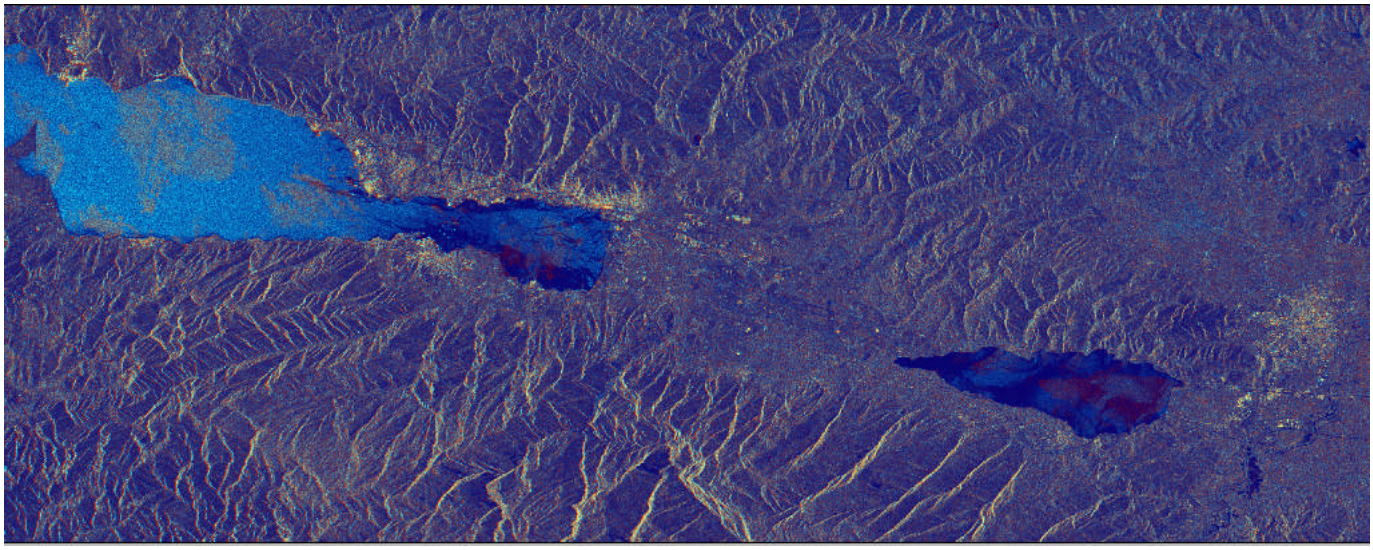

Image 19: *This image is obtained from the images of 13 August, 16 September 1999 and the second principal component of these two images.*

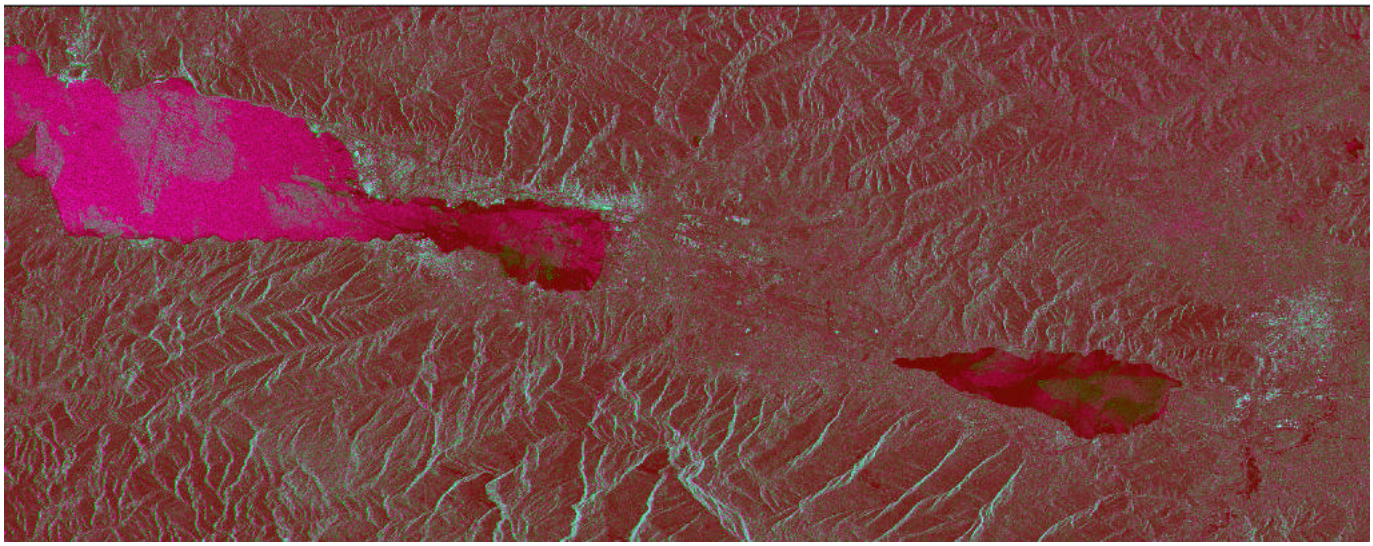

Image 20: *This image is obtained from the images of 13 August, 16 September 1999 and the second principal component of these two images. But in this case red color is given to the principal component image and green and blue colors are given to the images of 13 August, 16 September 1999 respectively.*

Multiplying the images of 13 August and 16 September generates image 21. Only the corresponding pixels with different brightness values give a different pixel value in comparison to the corresponding unchanged pixels in two images.

Image 22 is generated from the coherence image (red), division image (green) and the first principal component image (blue) obtained from the images of 13 August and 16 September 1999, whereas the Image 23 is generated from coherence image (red), the first principal component image (green) and the second principal component image (blue) of the images of 13 August and 16 September. In the Image 23 blue and cyan colors indicates the changes. In the Image 22 on the other hand green and magenta colors is the indication of change.

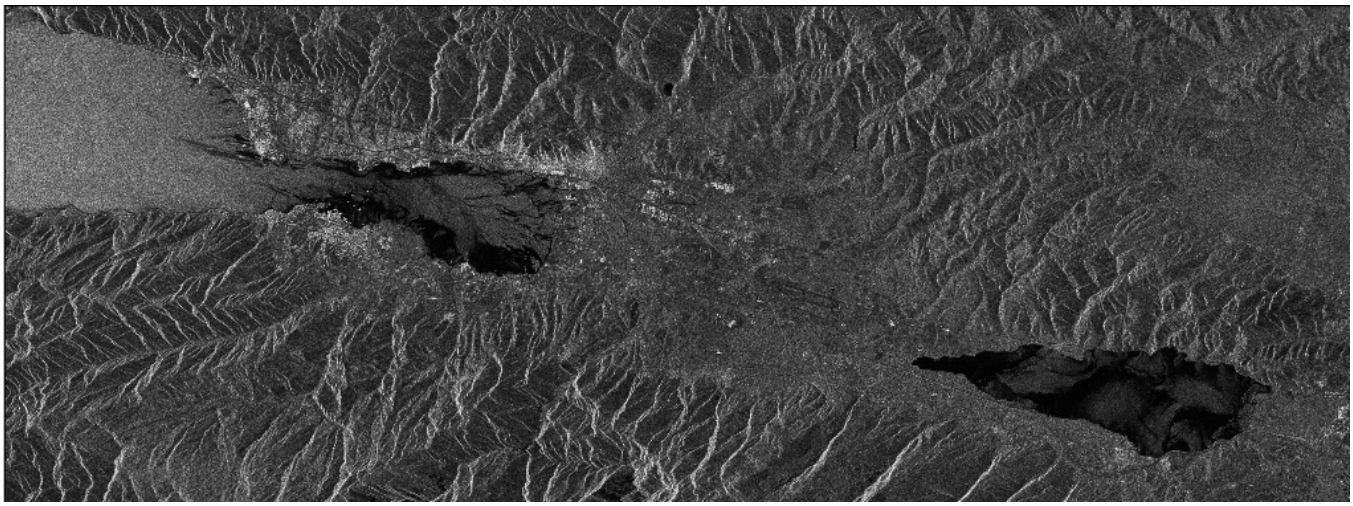

Image 21: *This image has been generated multiplying the images of 13 August and 16 September.*

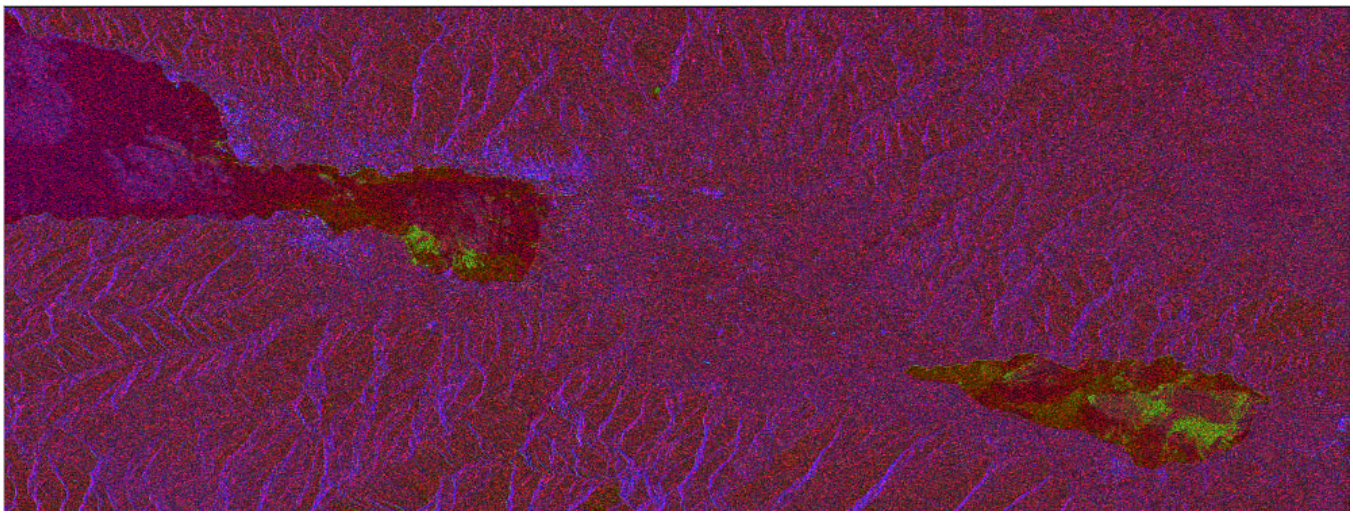

Image 22: *This image is generated from the coherence image (red), ratio image (green) and the first principal component image (blue) obtained from the* images of 13 August and 16 September 1999*.*

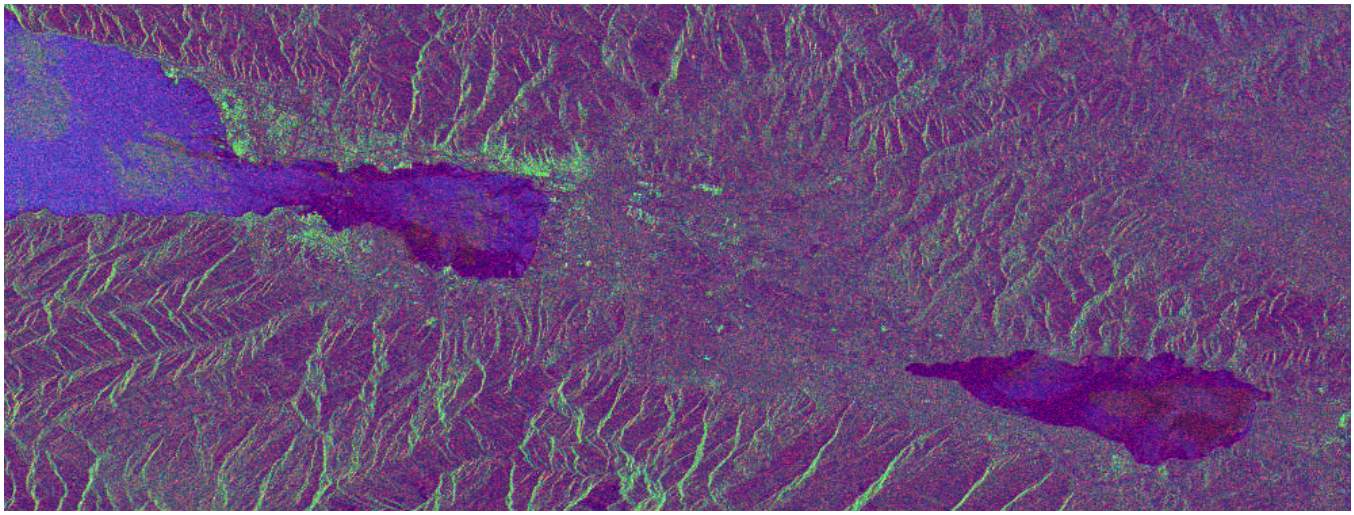

Image 23: *This image is generated from coherence image (red), the first principal component image (green) and the second principal component image (blue) obtained from the images of 13 August and 16 September.*

II) Interferometric SAR products

Above we inspected some optical and non-interferometric SAR products. Although most of these products can reveal the changes caused by the earthquake qualitatively, the rate and trend of deformation are still obscure. A very precise quantitative analysis of displacements is made possible through interpretation of interferograms produced for this purpose.

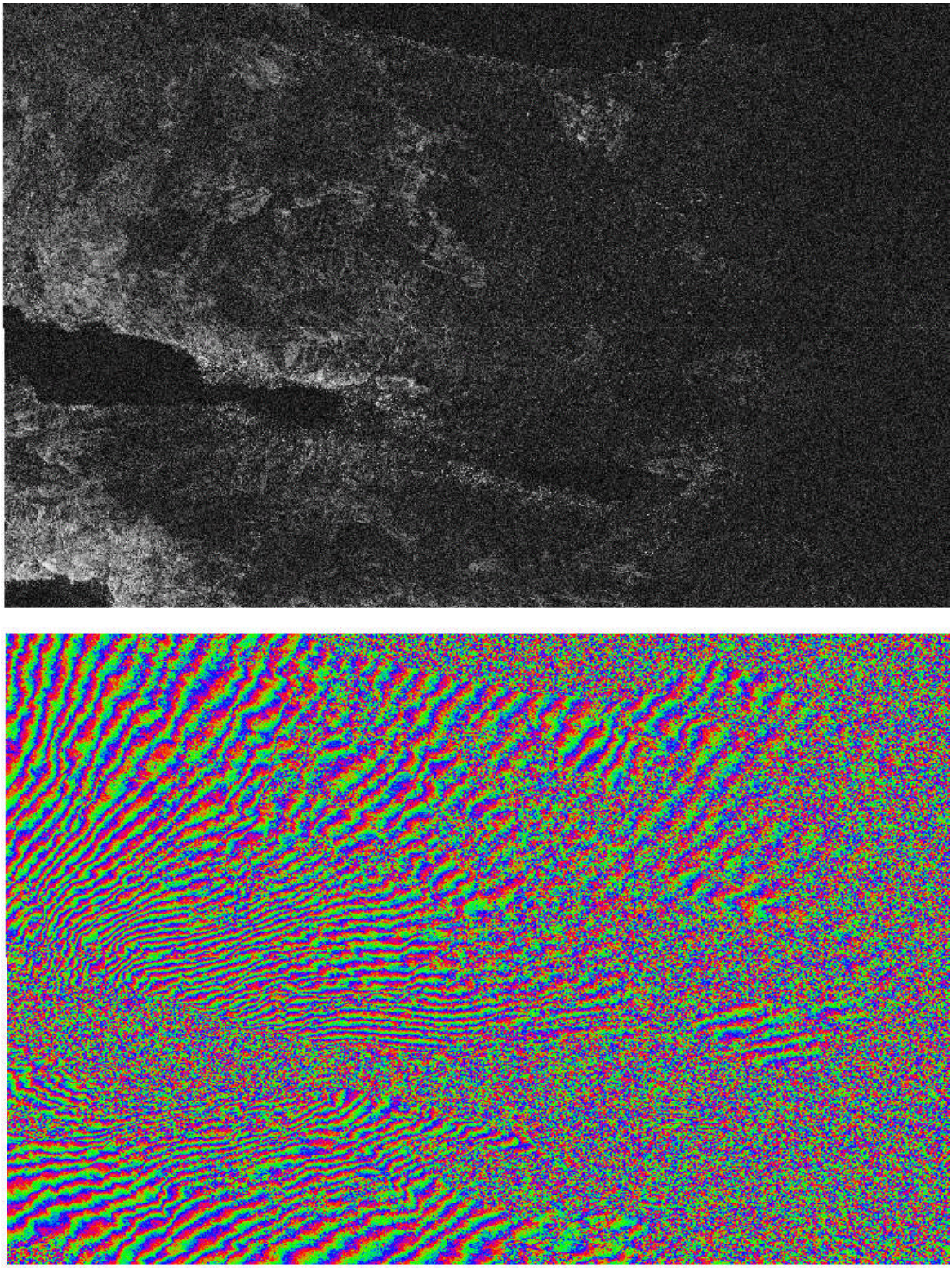

Image 24: *Top image is the coherence image generated from the SLCI ERS-SAR images of 13 August 1999 and 17 September 1999. The bottom image is the phase image generated from the same image pairs.*

Image 24 consists of two images. The top image is the coherence image generated in slant range mode from the SLCI ERS-SAR images of 13 August 1999 and 17 September 1999. The slant range projection mode matches the enhanced interferogram pixel by pixel. The bottom image is the enhanced interferogram generated from the same image pairs. Both the images are collected by ERS-2. The poor correlation can be distinguished in the area between the Lake Sapanca and the Izmit Bay. There is also poor correlation in the urban area around the Izmit Bay. The high density of the fringes in the mentioned areas is the indication of the highest replacement that can be the reason for poor correlation in the coherence image. In the Image 25 the phase image of the Image 24 is mapped on the intensity image of the SAR image of 13 August that is the master image of the SLCI pair. SAR images of 13 August 1999 shows the area 3 days before the quake and the image of 17 September 1999 shows the same area a month after the quake. The normal and parallel components of baseline for this image pair are 11.401m and 53.558m respectively. This is good case for generating a precise interferogram as well as DEM and the team succeeded to generate them.

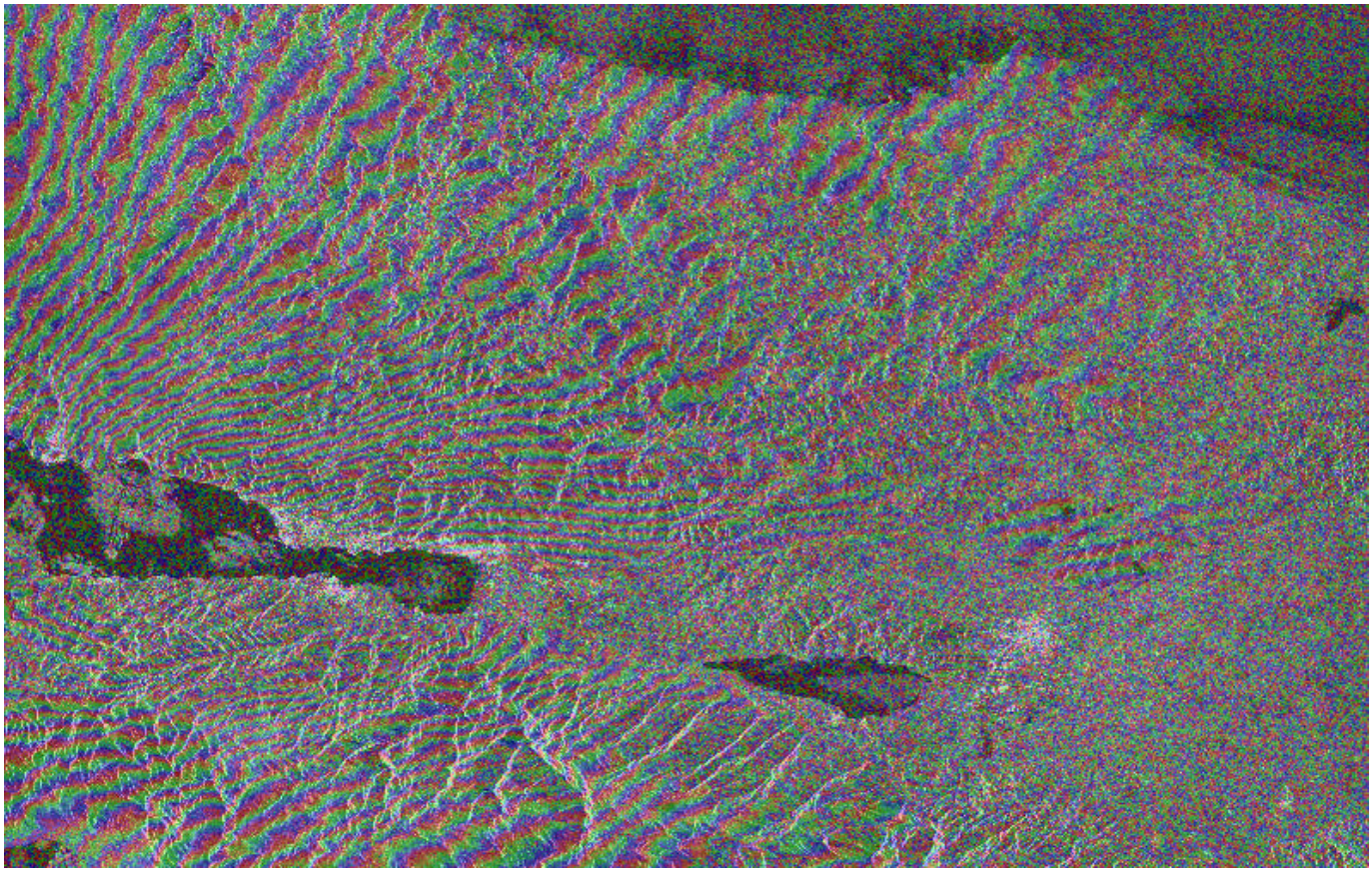

Image 25: *This image is generated by mapping the phase image of the Image 24 on the intensity image of the SAR image of 13 August that is the master image of the SLCI pair.*

Image 26 top is the coherence image generated from the SLCI ERS-SAR images of 17 September and 13 August 1999. The difference with the corresponding image of 24 is that in the image 26 we have displaced the master and slave images and generated a new coherence, phase images and interferogram. We have done this for all of the possible pairs and in Table 3 in Appendix B (appendB) the relevant baselines can be found. It can be seen easily that there is some difference between the baselines of a pair with the one generated when we changed the place of master and slave images. This is a point to be investigated in depth and find the proof for this difference. It will also be of concern to find the difference between the corresponding products precisely. The bottom image is the enhanced interferogram generated from the same image pairs. In the Image 27 the phase image of the Image 26 is mapped on the coherence image. Normal and parallel components of baseline for this image pair are 13.971m and 53.767m respectively.

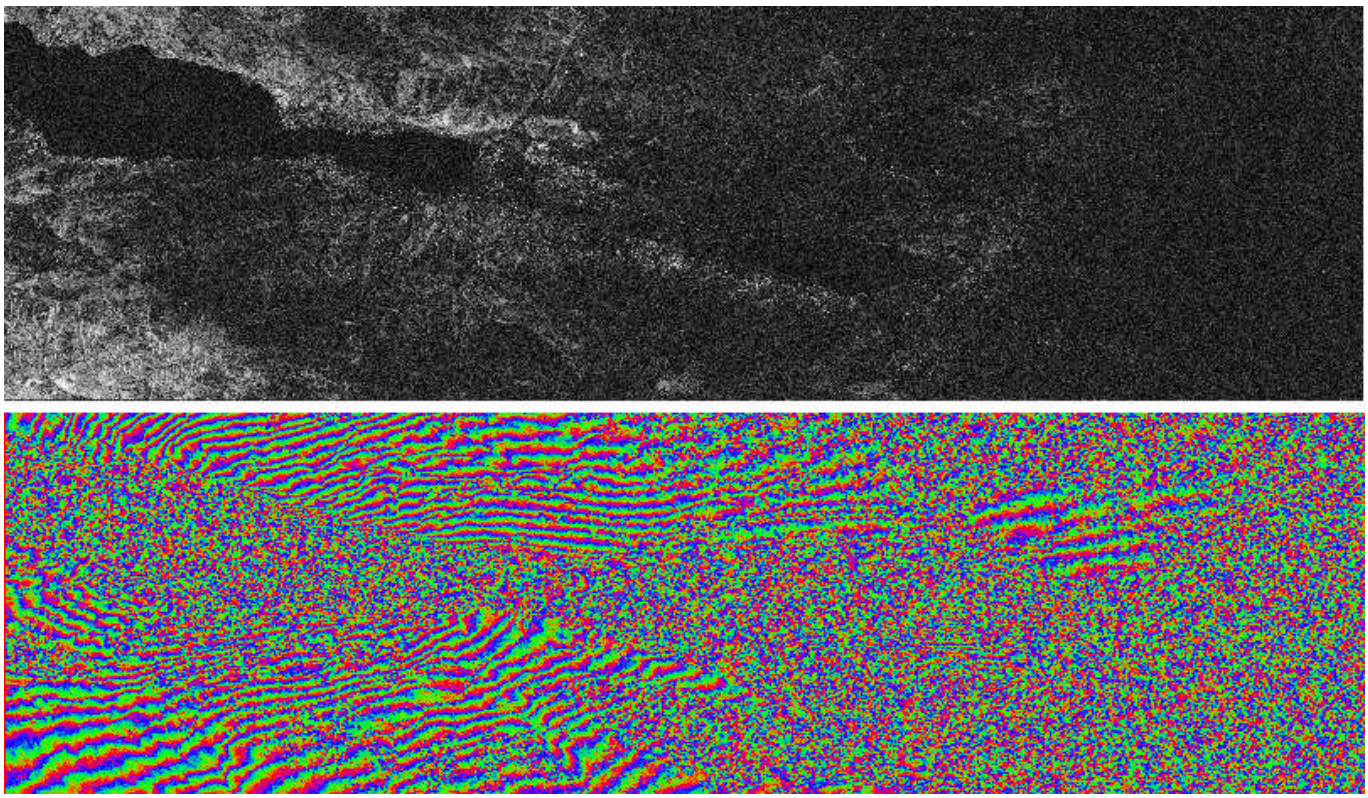

Image 26: *Top image is the coherence image generated from the SLCI ERS-SAR images of 17 September 1999 and 13 August 1999. The bottom image is the phase image generated from the same image pairs.*

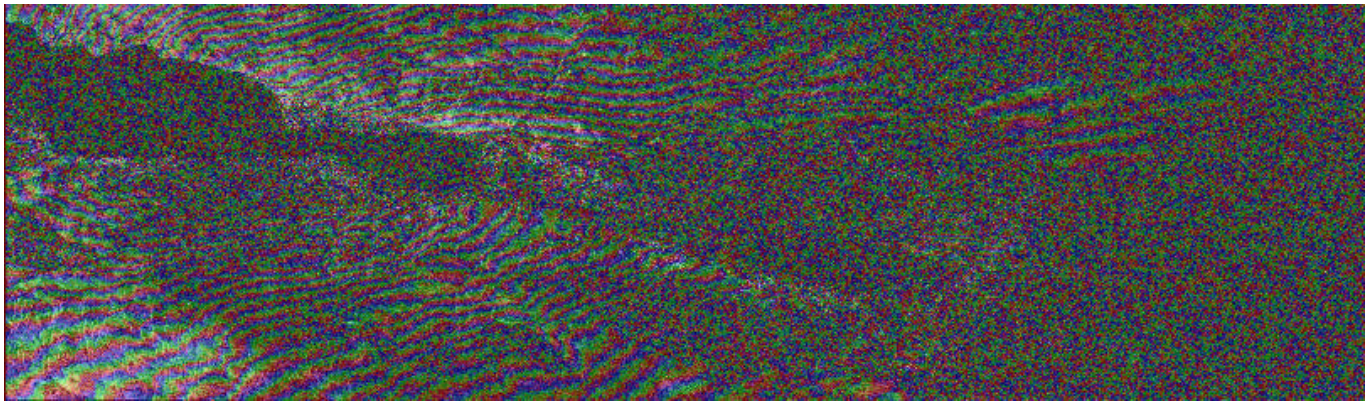

Image 27: *This image is generated by mapping the phase image of the Image 26 on the coherence image.*

Image 28 consists of two images including the coherence image on top and phase image in bottom. These images are generated in geocoded mode from the SLCI ERS-SAR images of 12 August 1999 and 16 September 1999. In geocoded projection mode the image is terrain corrected and re-sampled to a standard map projection that in this case is WGS84. Terrain corrected projection mode refers to a projection by which the height, coherence or any other data of the SAR image product is corrected for SAR image distortions such as layover and foreshortening. Both images are collected by ERS-1. The poor correlation can be distinguished in the area between the Lake Sapanca and the Izmit Bay. There is also poor correlation in the urban areas around the Izmit Bay. High density of the fringes in the mentioned areas indicates the highest displacement that can be the reason for the poor correlation in the coherence image. In the Image 29 the phase image of the Image 28 is mapped on the intensity image of the SAR image of 12 August that is the master image of the SLCI pair. SAR images of 12 August 1999 shows the area 4

days before the quake and the image of 16 September 1999 shows the same area a month after the quake. Normal and parallel components of baseline for this image pair are 121.640m and 67.725m respectively.

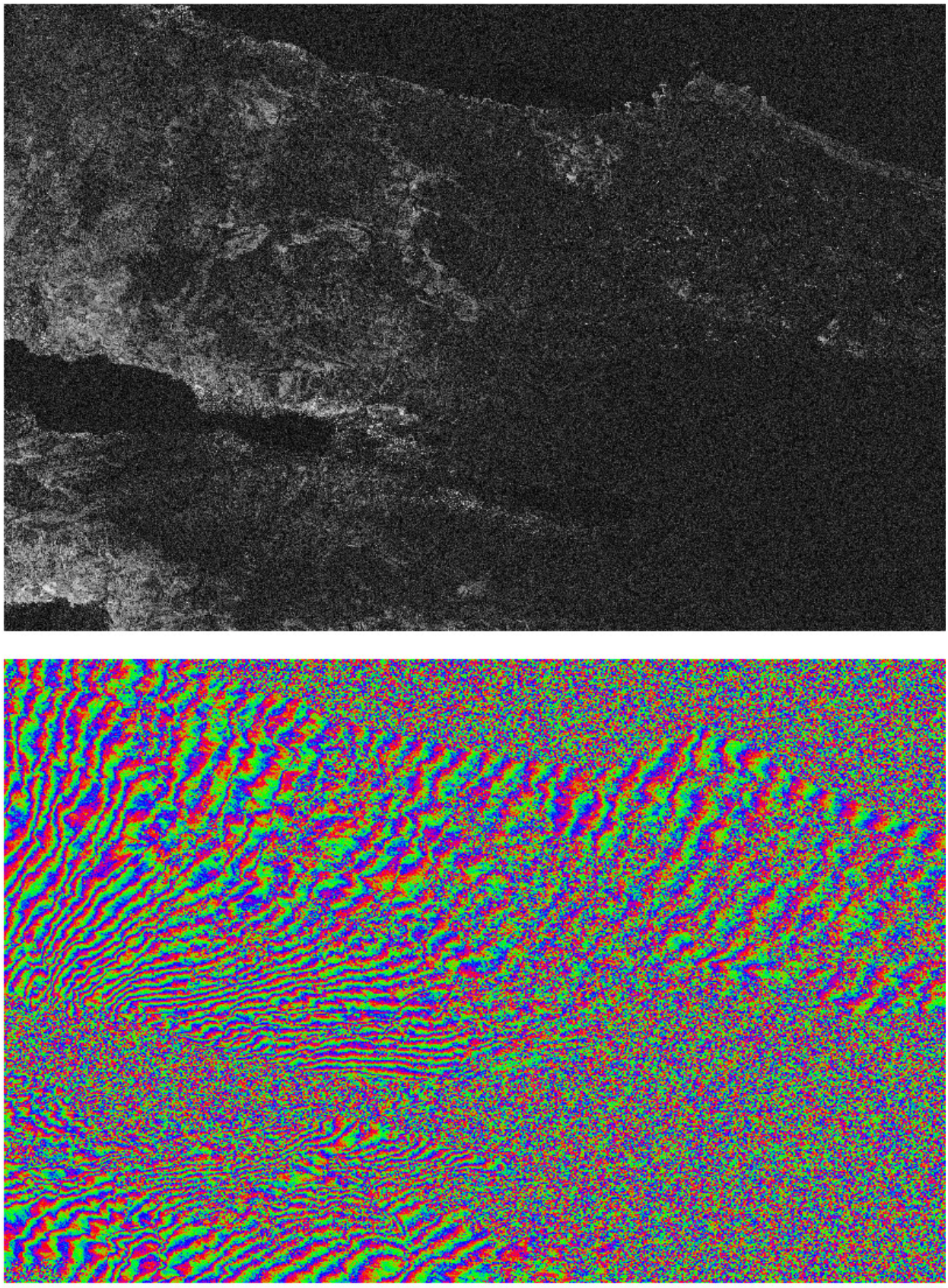

Image 28: *Top image is the coherence image generated from the SLCI ERS-SAR images of 12 August 1999 and 16 September 1999. The bottom image is the phase image generated from the same image pairs.*

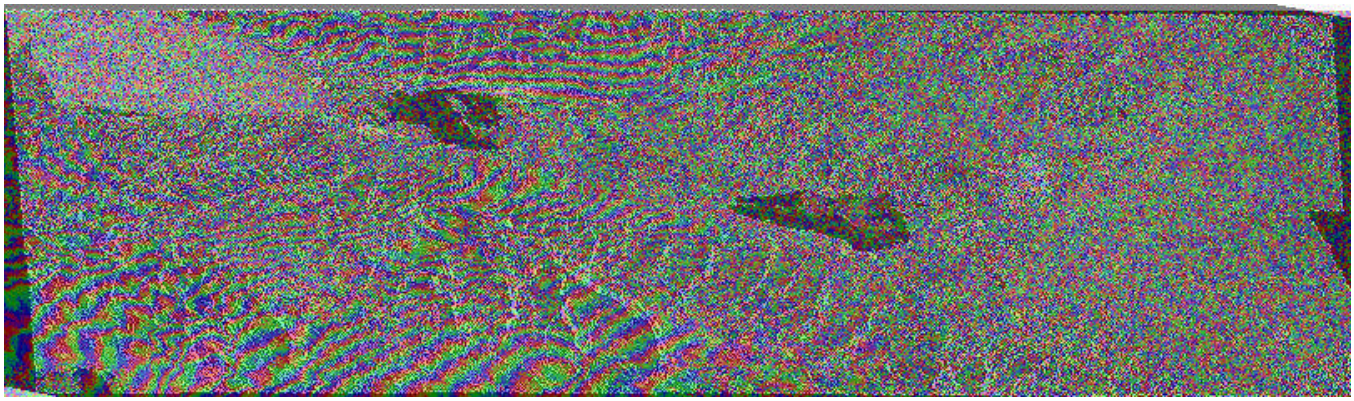

Image 29: *This image is generated by mapping the phase image of the Image 28 on the coherence image.*

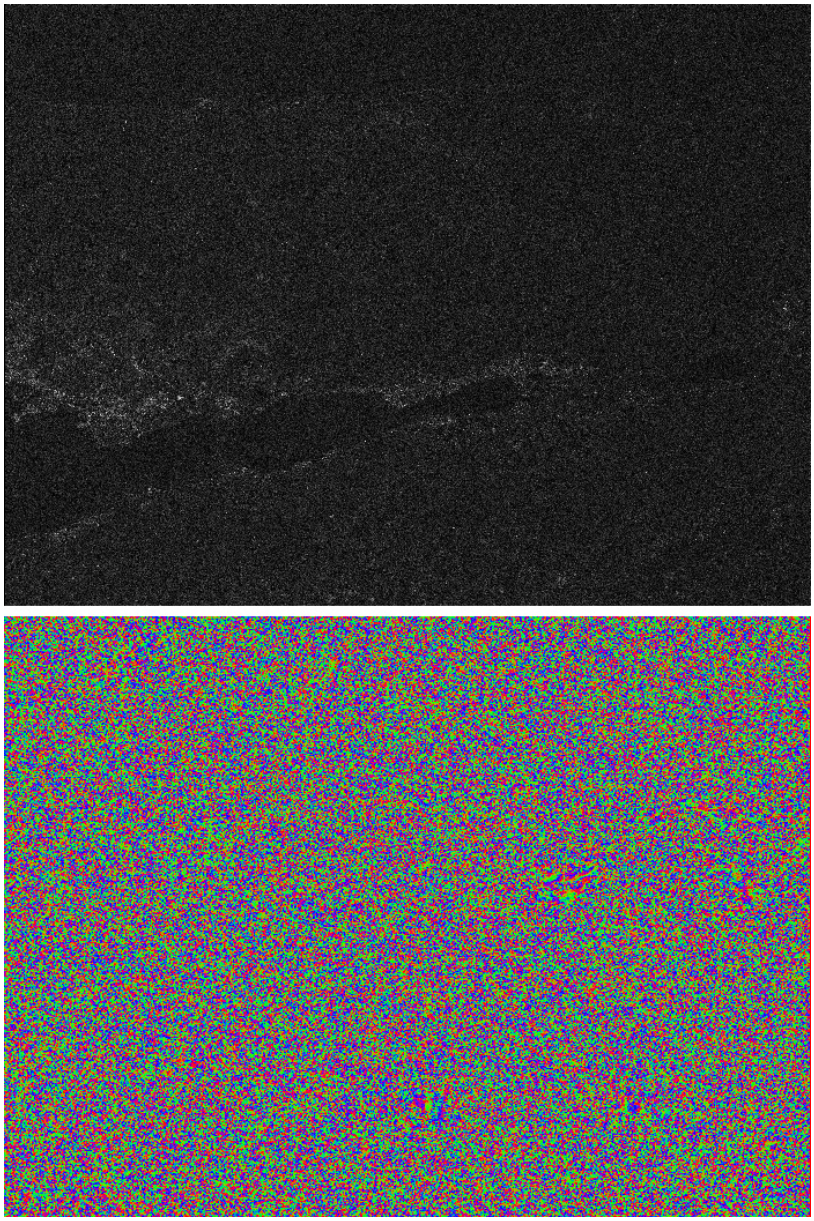

Image 30: *Top image is the coherence image generated from the SLCI ERS-SAR images of 24 April 1999 and 10 September 1999. The bottom image is the phase image generated from the same image pair.*

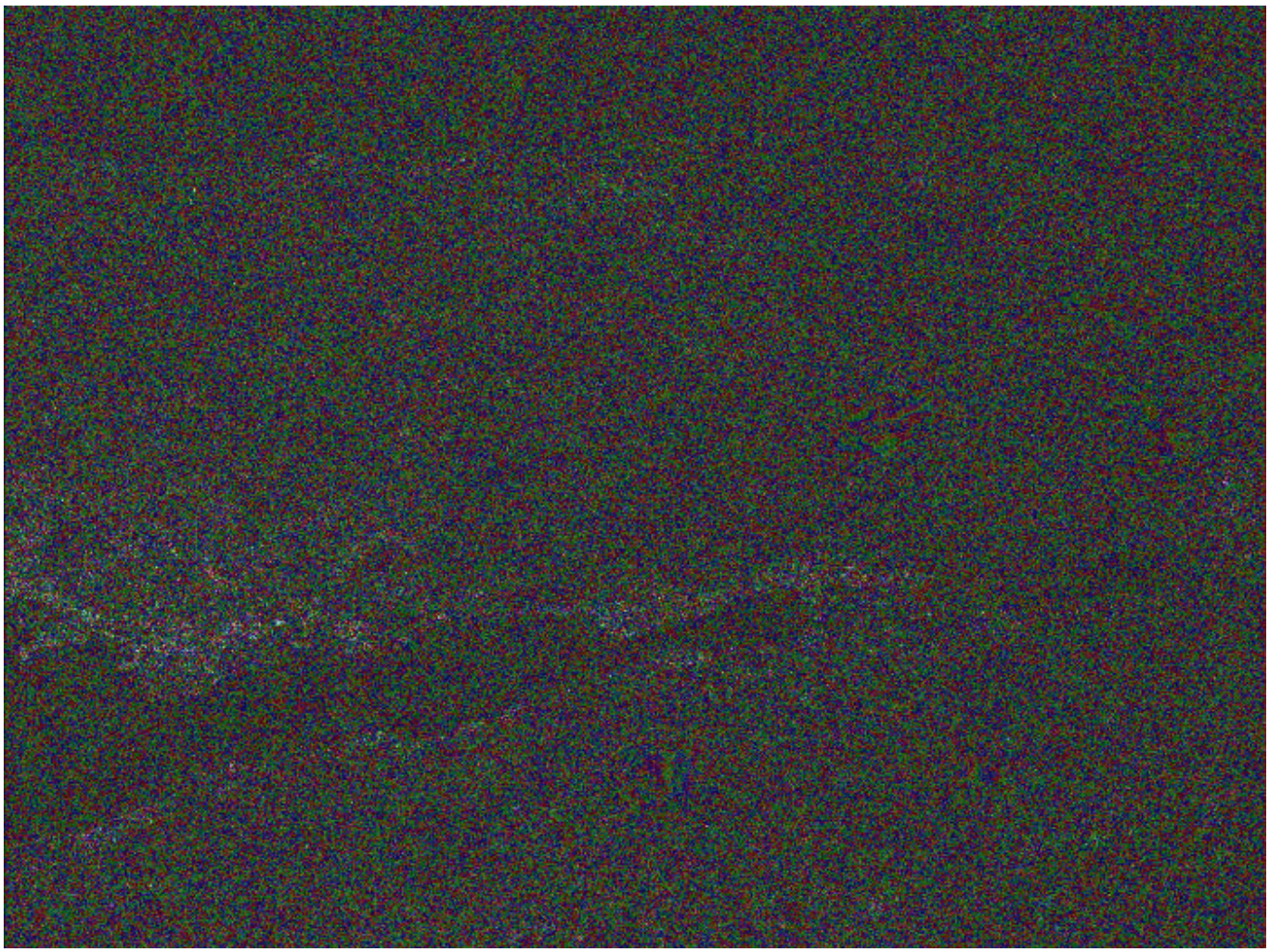

Image 31: *This image is generated by mapping the phase image of the Image 30 on the coherence image.*

Image 30 consists of two images including the coherence image on top and phase image in bottom.
These images are generated from the SLCI ERS-SAR images of 24 April 1999 and 10 September 1999. First image is collected by ERS-2 while the second image is acquired by ERS-1. Normal and parallel components of baseline for this image pair are 387.704m and 189.965m respectively. The high normal or perpendicular baseline causes an unfavorable coherence and phase image. In the Image 31 the phase image of the Image 30 is mapped on the coherence image. SAR image of 24 April 1999 shows the area nearly 4 months before the quake and the image of 10 September 1999 shows the same area 24 days after the quake.
Image 32 consists of three images including the coherence image on top and phase image in the middle and the corresponding interferogram in the bottom. These images are generated from the SLCI ERS-SAR images of 24 December 1998 and 25 August 1999. First image is acquired by ERS-2 while the second image is collected by ERS-1. Normal and parallel components of baseline for this image pair are 40.850m and 118.674m respectively. There is a good correlation between the two premier SLCI images and this can be seen from the coherence as well as the phase image clearly. SAR image of 24 December 1998 shows the area nearly 8 months before the quake and the image of 25 August 1999 shows the same area only 9 days after the quake. The horizontal surface displacement due to the earthquake is the evident characteristic of the Image 32 that is reflected by fringes.

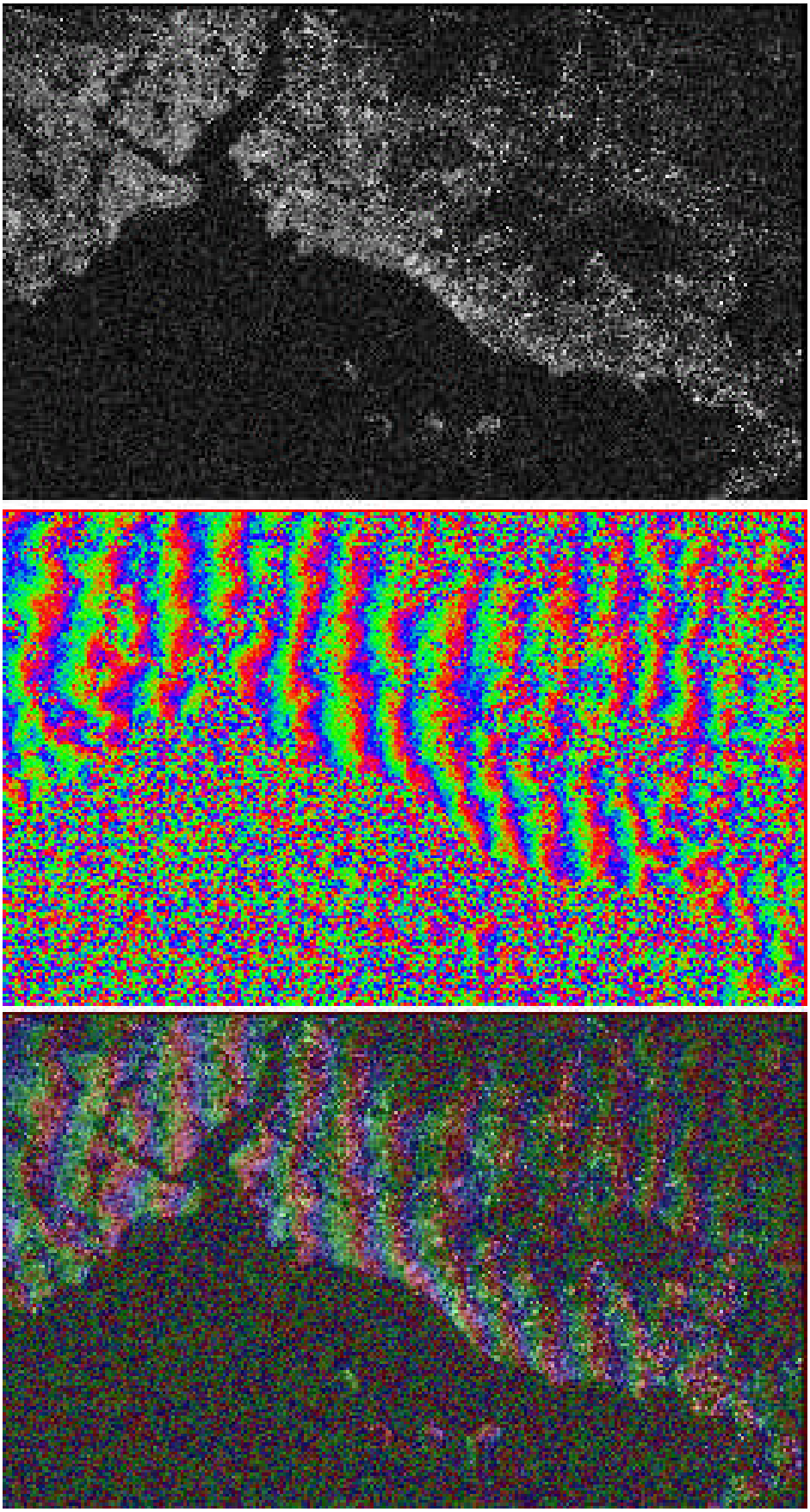

Image 32: *Top image is the coherence image generated from the SLCI ERS-SAR images of 24 December 1998 and 25 August 1999. The middle image is the phase image generated from the same image pair. Mapping the phase image on the coherence image generates the bottom image.*

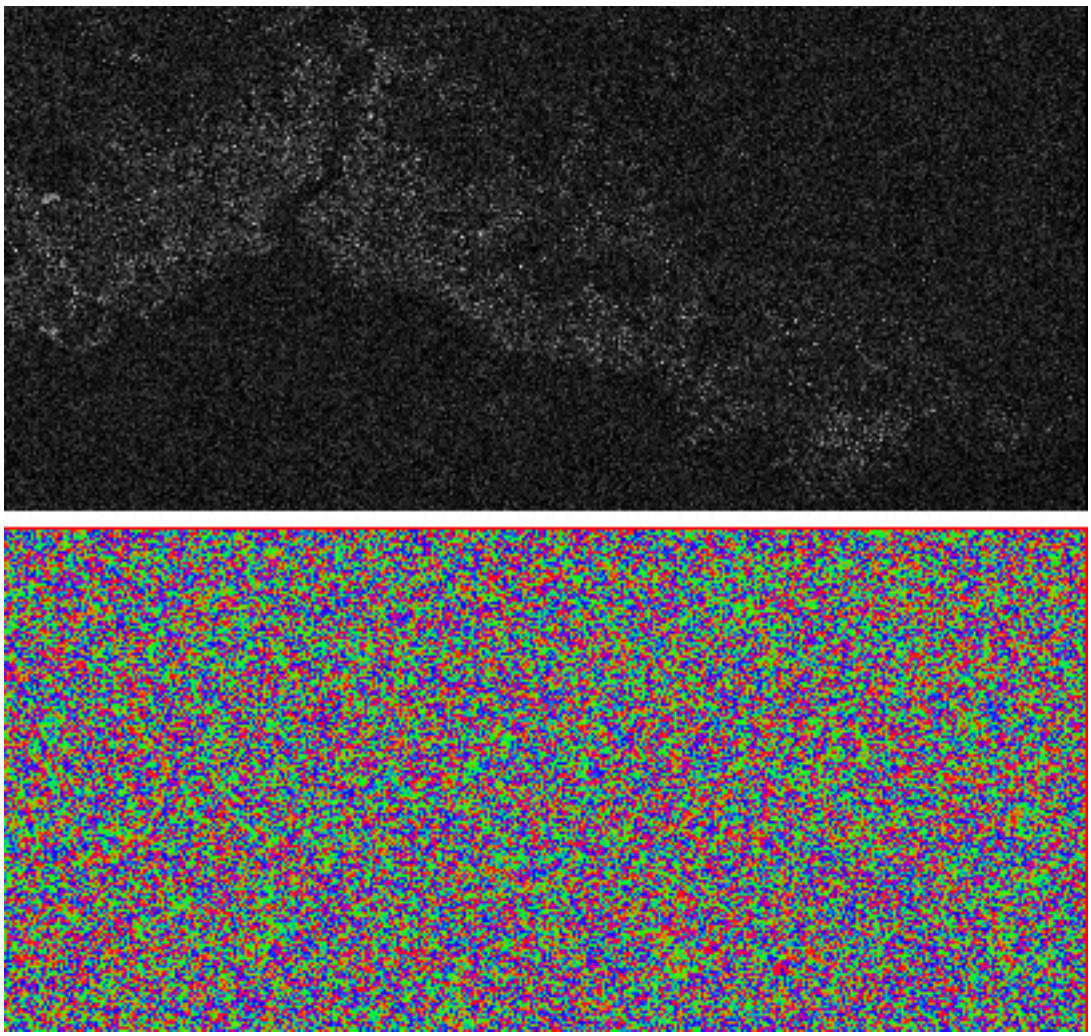

Image 33: *Top image is the coherence image generated from the SLCI ERS-SAR images of 24 December 1998 and 26 August 1999.*

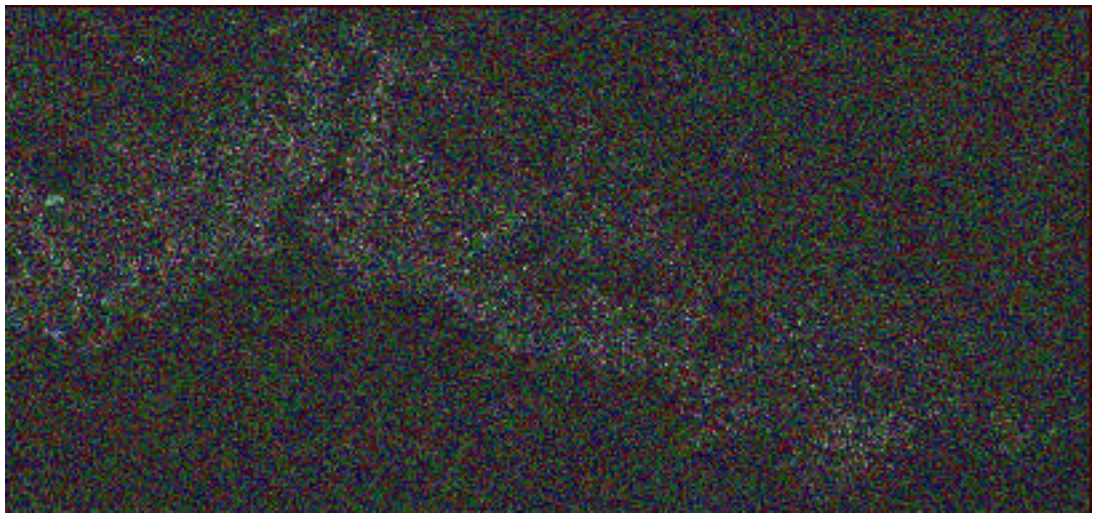

Image 34: *This image is the phase image of Image 33 mapped on coherence image.*

Image 33 consists of two images including the coherence image on top and phase image in bottom. These images are generated from the SLCI ERS-SAR images of 24 December 1998 and 26 August 1999. Both images are collected by ERS-2. Normal and parallel components of baseline for this image pair are 410.853m and 21.891m respectively. The high normal baseline causes a disqualified coherence and phase image. In the Image 34 the phase image of the Image 33 is mapped on the coherence image.
Image 35 consists of two images including the coherence image on top and phase image in bottom. These images are generated by geocoded projection mode from the SLCI ERS-SAR tandem images of 12 and 13 August 1999. The image of 12 August is collected by ERS-1 while the other image is acquired by ERS-2. Normal and parallel components of baseline for this image pair are 224.190m and 91.097m respectively. The correlation in the coherence image except for the areas around the Izmit Bay and east of the Lake Sapanca is considerable. The phase image shows this apparently. This may be interpreted as the sign of early surface disturbances started prior to the earthquake main shocks. In the Image 36 the phase image of the Image 35 is mapped on the intensity image of the image of August 12. Image 37 shows the height image or the DEM of the area.

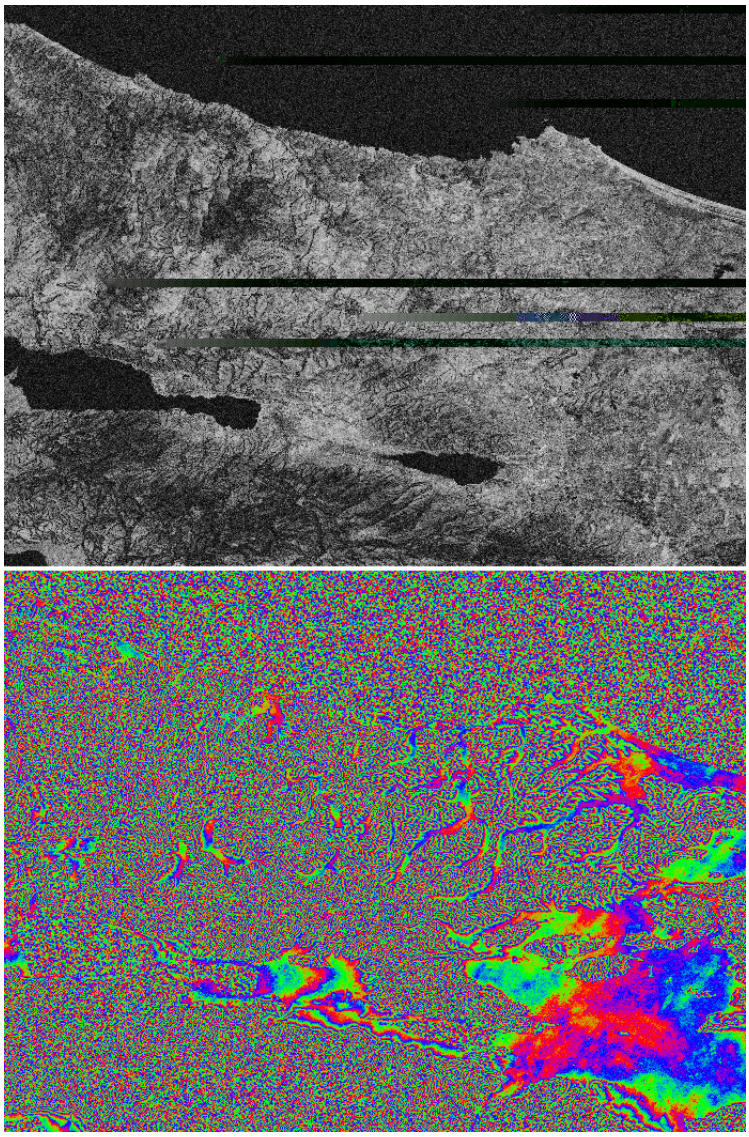

Image 35: *Top image is the coherence image generated from the SLCI ERS-SAR tandem images of 12 and 13 August 1999.*

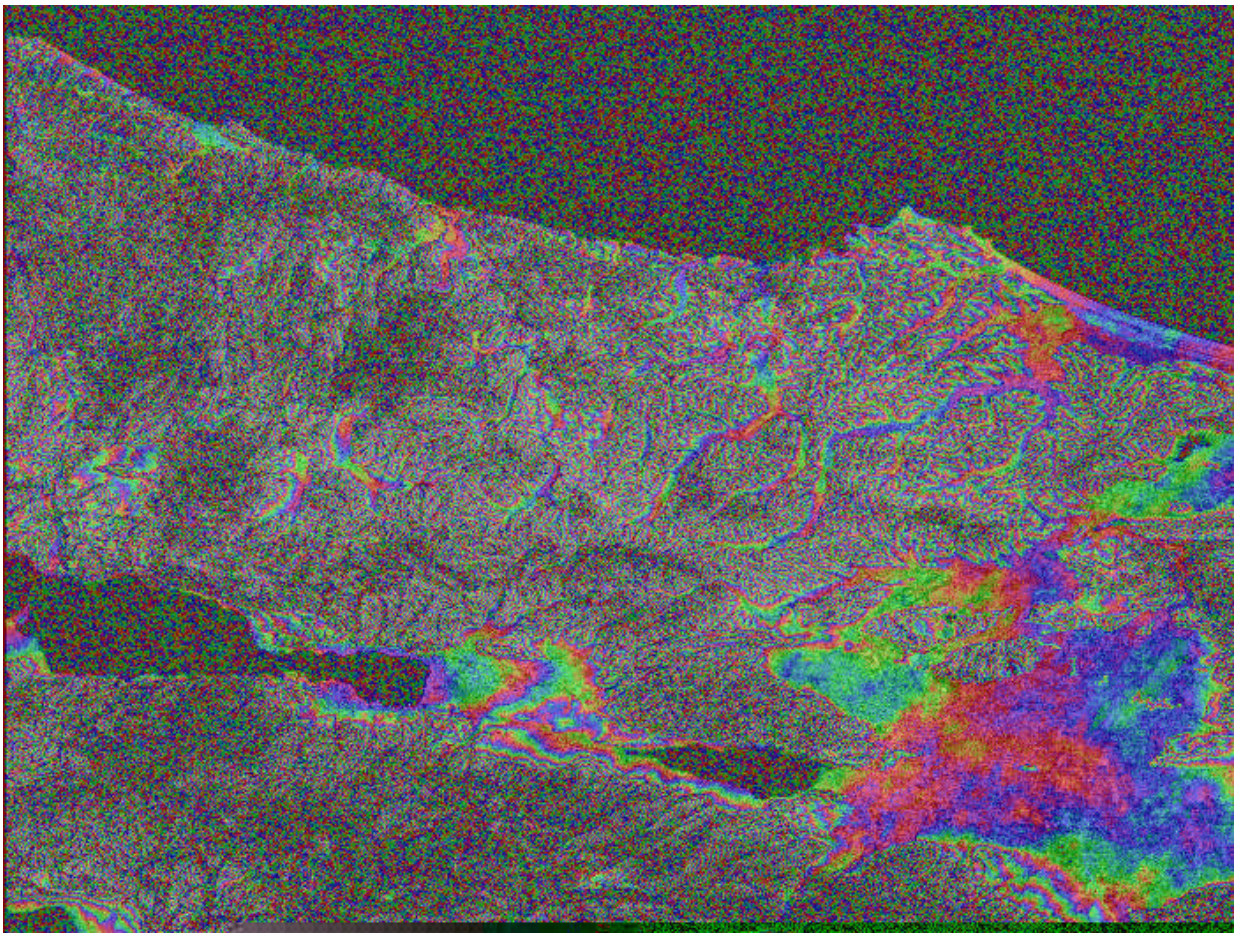

Image 36: *This image is generated by mapping the phase image of the Image 35 on the intensity image.*

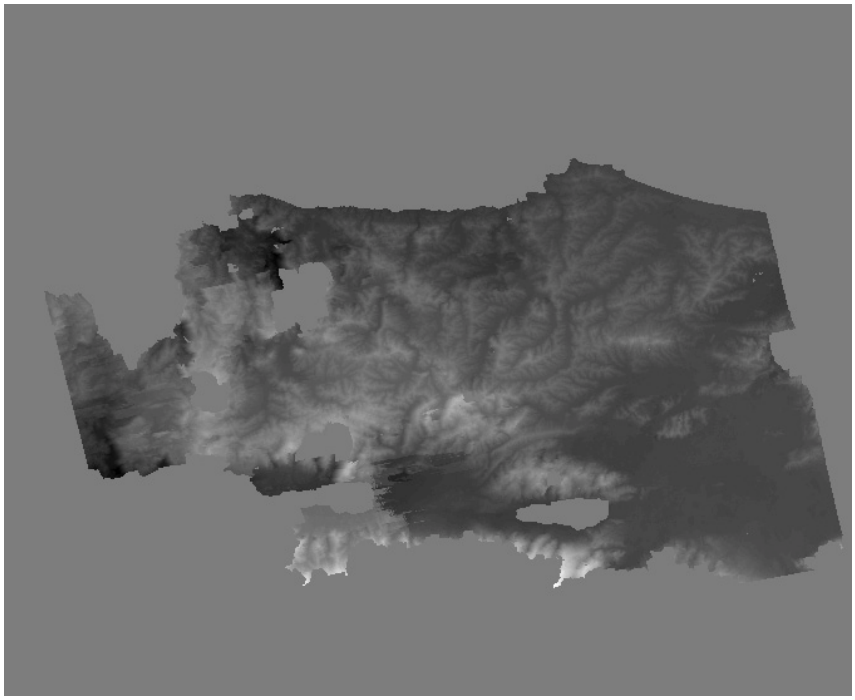

Image 37: *The height image of the tandem images of 12 and 13 August 1999.*

Image 38 consists of two images including the coherence image on top and phase image in bottom. These images are generated by geocoded projection mode from the SLCI ERS-SAR tandem images of 10 and 11 September 1999. Both the images are collected by ERS-1. Normal and parallel components of baseline for this image pair are 182.313m and 73.239m respectively. The decorrelation in the coherence can be distinguished in the areas around the Izmit Bay and east of the Lake Sapanca. The phase image shows this apparently. This is a point for further investigation that whether this decorrelation is due to the shocks occurred during the later days. In the Image 39 the phase image of the Image 38 is mapped on the intensity image of the image of September 10. Image 40 shows the geocoded interferogram and image 41 shows the height image of the area.

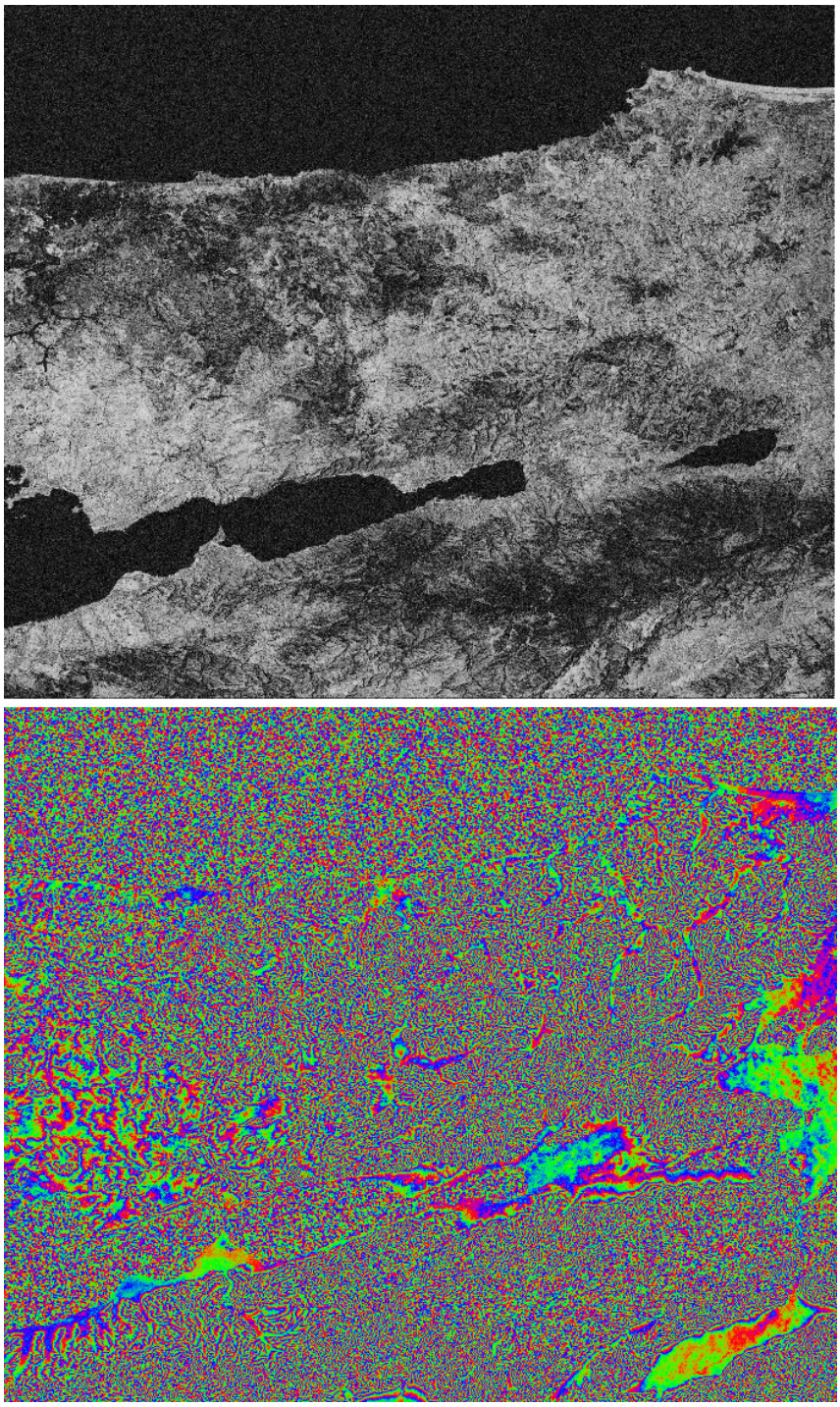

Image 38: *Top image is the coherence image generated from the SLCI ERS-SAR tandem images of 10 and 11 September 1999.*

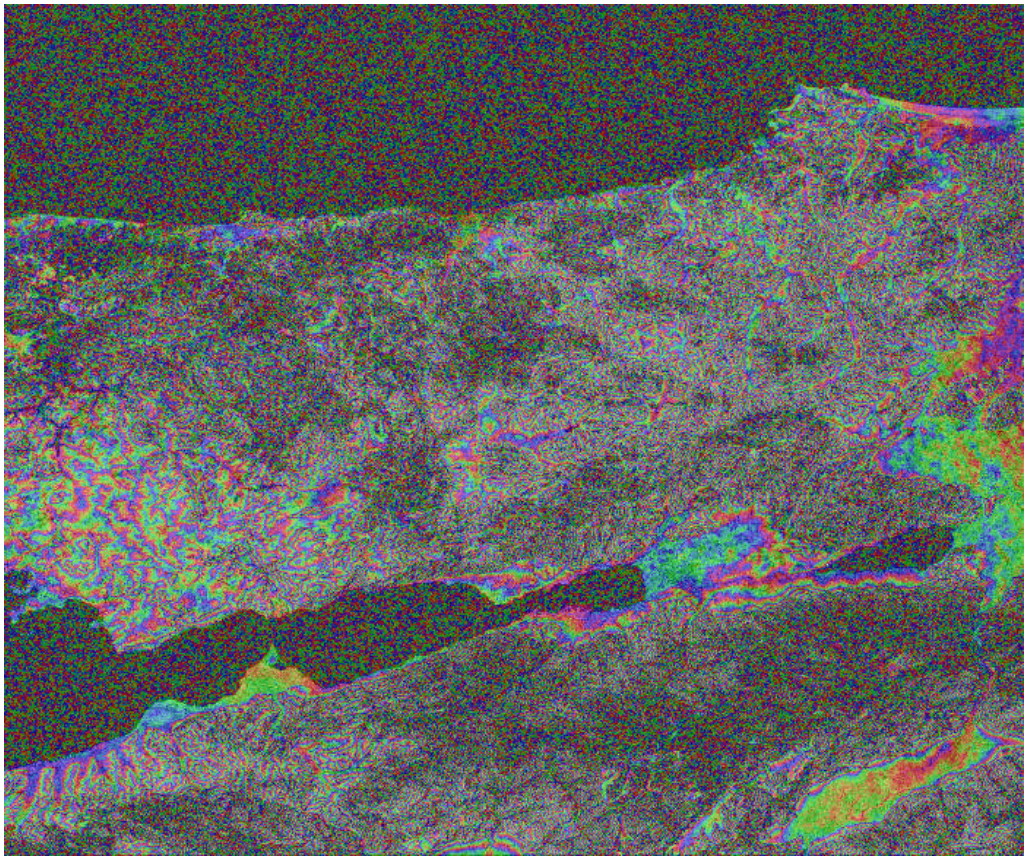

Image 39: *This image is generated by mapping the phase image of the Image 38 on the intensity image.*

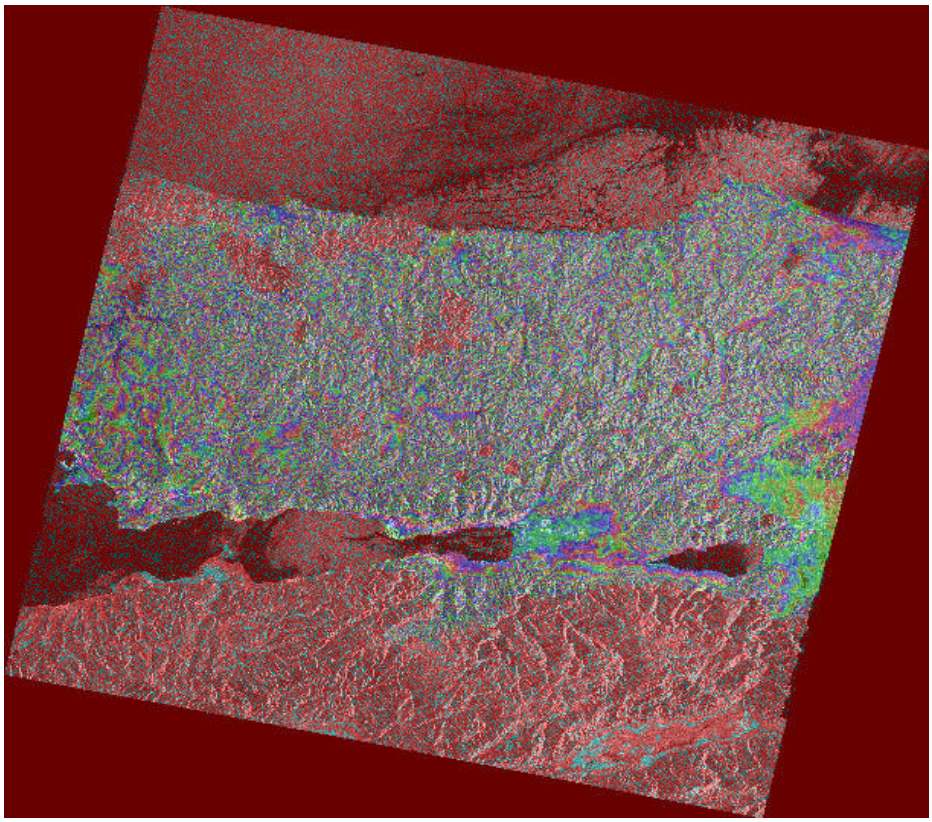

Image 40: *This image is the geocoded interferogram of the Image 38.*

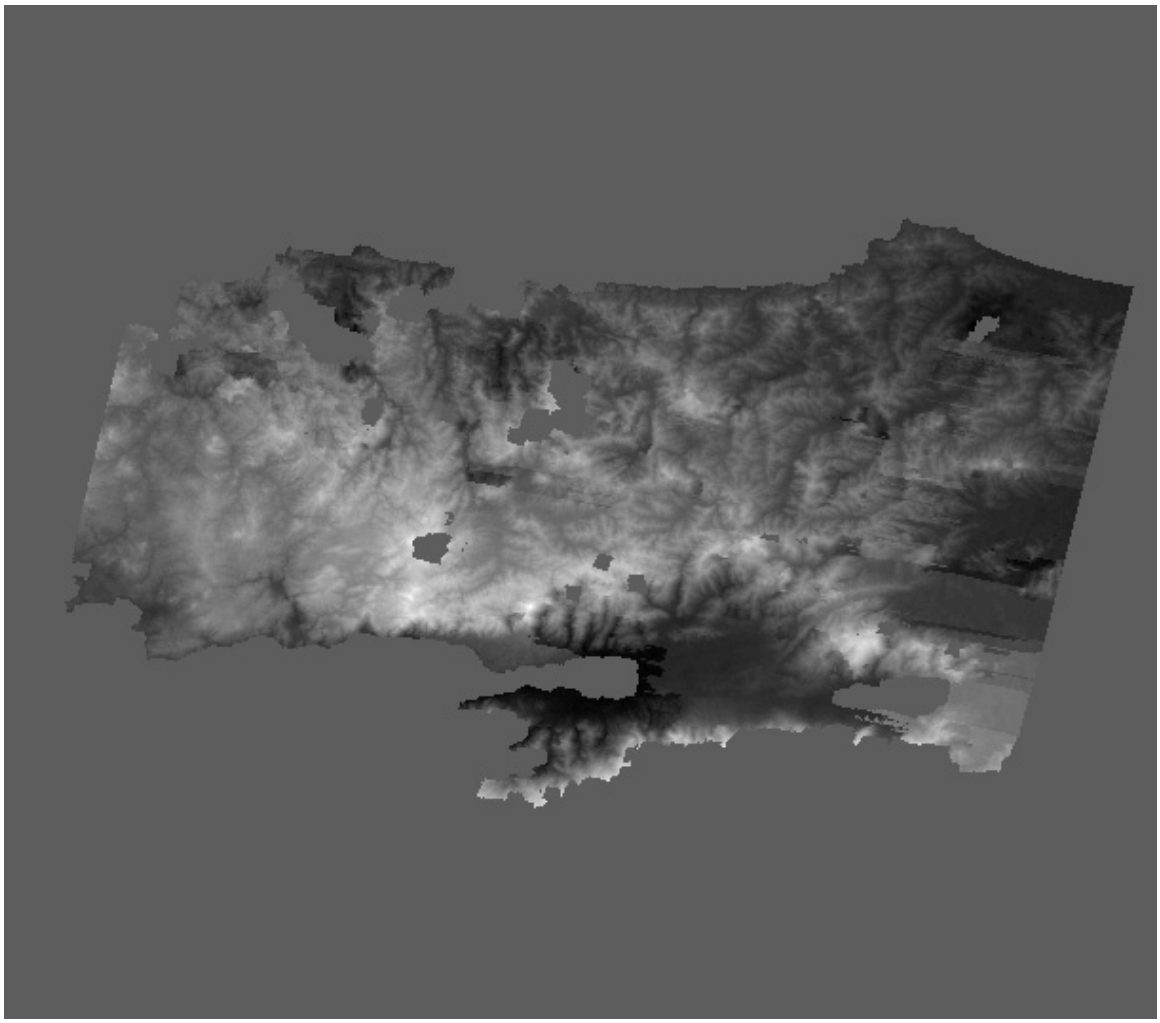

Image 41: *The height image generated from the tandem images of 10 and 11 September 1999.*

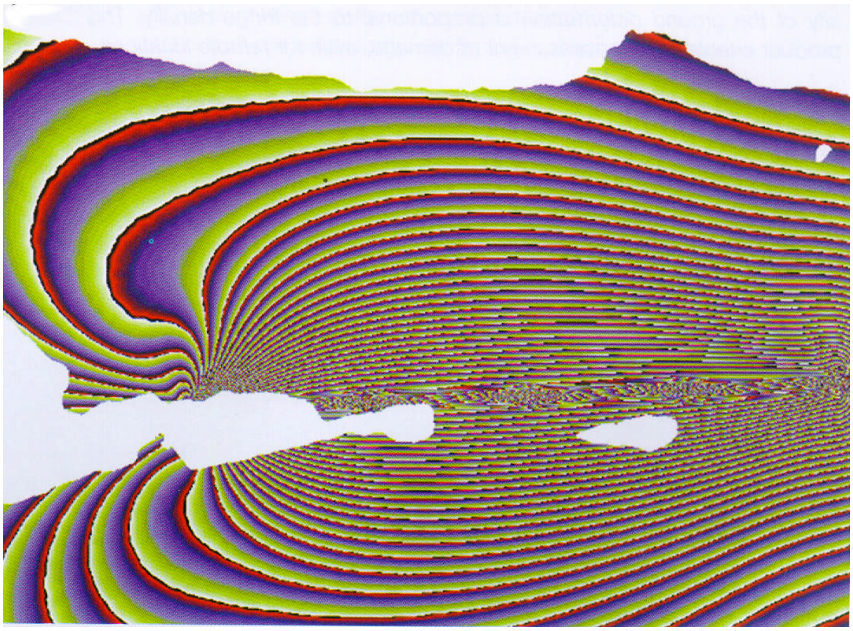

Image 42: *theoretical deformation model for the area struck by the quake, which is derived from geophysical data (source ESA).*

INFORMATION ANALYSIS

The data applied to generate SAR differential interferograms show ground surface deformation in an area extending from Istanbul to the east of Lake Sapanca. The density of the fringes is proportional to the degree of change and consequently the rate of damage caused by the earthquake. Results derived from phase interferograms show the consistency of the outputs with the theoretical deformation model, which is derived from geophysical data (Image 42). According to the geophysical data interpretation the rupture occurred along an east-west trending strike-slip fault that caused a predominant horizontal displacement of the ground surface. In the case of Izmit quake 36 fringes can be counted in the northern area of Izmit Bay in Kocaeli Province and 24 fringes in the northern area. This means that along the northern area there is 100.8cm displacement and 67.2cm displacement in southern area in the satellite s viewing direction. The horizontal component of these displacements can be computed simply given the viewing incidence angle of ERS satellites that is a fixed amount of 23 degrees. The direction of the horizontal displacements in two sides of the rupture is apparent.

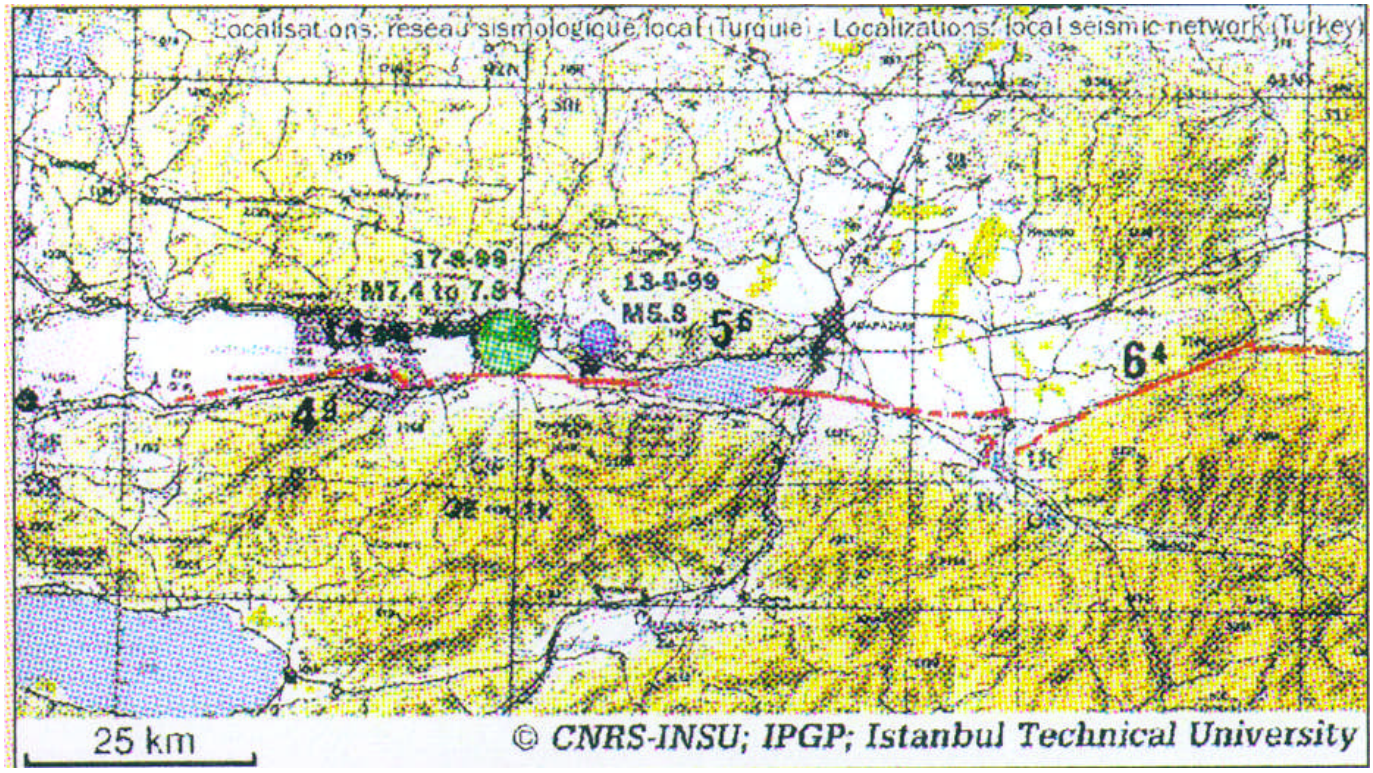

Image 43: *Fault map of the study area.*

Comparison of the TM data of region before and after the quake supports the acquired information from SAR interferometry for precise validation. However, this requires to be combined with parameters such as topographic, land-cover and land-use maps, for correct estimates. Investigating and detecting the eventual changes on the region using the image processing systems provides the data for incorporation to a GIS that shows the potent places.

Change detection of the area devastated by the quake using two Landsat TM imagery of the area before and after the quake reveals interesting differences. One of these changes can be attributed to the water transgression in a vast area 0.605sq.km in the northern coast of Izmit Bay next to Derince. While the TM image before the quake goes to 27 March 1999, the second image shows the Izmit area a day after quake.

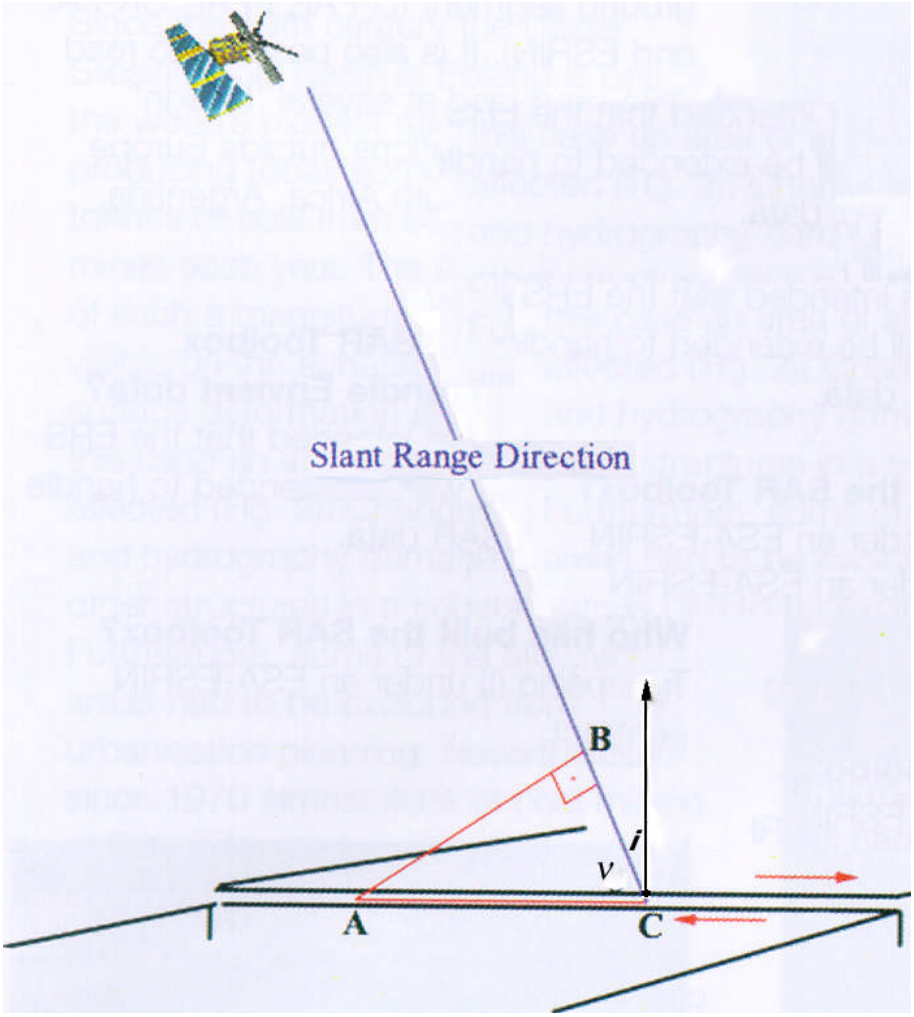

Image 44: *In the case of Izmit quake since it was almost horizontal movement that occurred in east-west direction parallel to satellite's observation, one observation is sufficient to define the spatial displacement vector. The geometry is seen above. From the image calculating cos v gives the surface displacement, where v=67 deg. and BC is the displacement in satellite's direction.*

Using SAR interferometry the displacement originated by earthquakes can be qualified. To define the spatial displacement vector generally three measurements are needed. Consequently three interferograms from different viewing angles are required. Practically SAR data from ERS ascending and descending passes would provide two of the three interferograms. Both historical data and tectonic analysis of the area may retrieve the third observation. However, in the case of Izmit quake since it was almost horizontal movement that occurred in east-west direction parallel to satellite's observation direction, one observation is sufficient. The displacement in the northern area is derived to be 258cm whereas it is 167cm in the southern area.

Alternatively, satellite orbit has a key role in successful application of SAR interferometry. Better results for differential interferometry highly depends on the smaller separation between two observations that means a smaller normal baseline. Generally a normal baseline larger than 400m is usually not suitable for interferometry due to decorrelation or sampling the slopes. On the other hand the baselines smaller than 40m may not be suitable for DEM generation since slopes will be under-sampled. But this data will be very good for differential interferometry where height information is to be removed. Small baselines are optimal to preserve the coherence while in this case the influence of the ground topography in the interferogram becomes negligible. These statements were proved in the Izmit case study. The altitude

color-coded and shaded digital elevation maps generated from ERS image pairs show the morphological and tectonic features in the area.
However, it has been appeared that short-term variations in the atmosphere and ionosphere can sometimes alter the fringe pattern. Changes in the earth surface properties can also induce the shift of interference fringes, even though the ground does not move actually. Such effects can complicate the interpretation of radar interferograms. But on the other hand these secondary influences represent features of the earth that are also of interest.

PROMISING RESULTS

The results of such a study help to establish an estimation model. Although the results are still need to be tested and proved by sufficient ground truth data, considerable interest is seen in the results of the project. They can be used for sustainable development of region and risk management as well. Recommending the instructions based on the results of the project to the respective authorities, they can take convenient and informed actions that may prevent the damages or reduce the effects and losses. The users of these results would be governmental and non-governmental organizations involved in the application of lands and natural resources for the issues such as land use planning, resource and environmental management, risk management as well as the relevant research and investigation programs.
There is a wide range of SAR interferometry applications that can be grouped into four areas including precision calibration, elevation mapping, land deformation, and super-sensitive change detection. An increasing number of applications have become feasible, and more are being investigated. Among the most exciting new applications of SAR interferometry is the two-dimensional mapping of large-scale surface deformation with very high precision. These deformation maps are used to detect and monitor Earth disasters including land deformation due to earthquakes, crustal movements, land slides, volcanic activity, mining and water extraction activities. Another interesting area of research is the use of phase coherence for classification and change detection.
Would SAR interferometry be able to detect the early indications needed to predict earthquakes and volcanic activities? None can be sure on this yet and presently it is an unrealistic matter but the hopes grow day by day. In scientific research each new tool reveals unprecedented issues that disclose crucial facts and deepens our perception of fundamental principles. Undoubtedly SAR interferometry does the same for the study of our solid but ever changing planet.

SUGGESTIONS AND EXPLANATIONS

- Since most of the analysis in this research has been based on the earth space data, to validate and completion of the analysis and the final results a field check by the investigators is needed.
- Due to inaccessibility of the information and records of the quakes in the region (especially from early 1998 to 17 August 1999) the discussions and analysis about some of the derived results from interferograms and the relevant products is tentative. This can be improved by a field check.
- The geological and structural information on the region was not sufficiently accessible and as a result for consistency of the outputs with the region’s tectonic when it was needed, the investigators have been acted conservatively and generally to avoid the errors.
- Although the investigators are convinced that the results of this research to achieve a prediction model is not sufficient, they believe that implementing the studies such as the present study based on continuos satellite monitoring and comparison of the different interferograms and integration of the results with other related tectonic, seismologic and geophysical data of any quake prone area in the world would make this possible.
- Due to the systematic and unforeseen problems and limitations during the term of the implementation of the project the investigators didn’t succeed to sufficiently and profoundly work out some cases and matters. Consequently they believe that further work and study should be carried out in this concern to find more supporting evidences for the project. In this regard they appreciate and welcome any further assistance and support from the relevant and interested people and organizations.

ACKNOWLEDGEMENT
The investigators give their kindest thanks to ESRIN and ESA for providing them with the needed data and software for the project as well as IRSC for providing the required hardware, software and continued supports.

Investigators biography

Parviz Tarikhi, born in 1960, is a researcher specializing in space science and technology based in Iran. He received the B.Sc. degree in Atomic Physics from Tehran University in 1991, and M.Sc. degree in physics from the Knightsbridge University, UK in April 1999. Presently he is a distance learning scholar for a Ph.D. degree in physics with Knightsbridge University, UK.
Working in the Iranian Remote Sensing Center since 1992, he has been involved in the research and development issues and projects of the applications of space science and technology.
His present research interests include holography for 3-D modeling of the land features and SAR interferometry for estimating the surface displacements and change detection.

Muhammad Morabbi, born in 1953, is a Remote Sensing technology application specialist in the Geology, Marine and Water Resources Division in the Iranian Remote Sensing Center. He received a B.Sc. degree in Geology from Tabriz University in 1987, and M.Sc. degree in Geology from Idaho State University, USA in 1981.
His present research interests include sea surface temperature, ocean color study, water pollution as well as geological dynamic studies through space radar interferometry.